Significant influence of oxygenated volatile organic compounds on atmospheric chemistry analysis: A case study in a typical industrial city in China

Jingwen Dai [a], Kun Zhang [a, *], Yanli Feng [a], Xin Yi [a], Rui Li [a], Jin Xue [a], Qing Li [a], Lishu Shi [a], Jiaqiang Liao [a], Yanan Yi [a], Fangting Wang [a], Liumei Yang [a], Hui Chen [a], Ling Huang [a], Jiani Tan [a], Yangjun Wang [a], Li Li [a, *]

[a] School of Environmental and Chemical Engineering, Shanghai University, Shanghai, 200444, China

Correspondence: Li Li (Lily@shu.edu.cn) and Kun Zhang (zk1231@shu.edu.cn)

Abstract

Oxygenated volatile organic compounds (OVOCs), an important subgroup of volatile organic compounds (VOCs), are emitted directly or formed secondarily through photochemical processes. They play a crucial role in tropospheric chemistry as ozone (O_3) precursors. However, due to measurement limitations, the influence of OVOCs on O_3 formation has often been underestimated. In this study, 74 VOCs (including 18 OVOCs) were measured at five representative stations (urban, suburban, industrial, upwind, and downwind stations) in Zibo, an industrial city in the North China Plain. The VOCs level in Zibo (44.6±20.9 ppb) is in the upper-middle range (> 32 ppb) compared to previous studies conducted in most Chines cities, with OVOCs contributing for 30.0%~37.8%. The average O_3 formation potential in Zibo is 410.4±197.2 µg m^{-3}, with OVOCs being the dominant contributor (31.5%~55.9%). An observation-based model (OBM) was used to access the contributions of chemical production ($R_{NetProd}$) and emissions/transport ($R_{Emis\&Trans}$) to individual OVOC. Daytime (8:00-18:00 LT) $R_{NetProd}$ is the highest at the urban site (5.9 ppb h^{-1}), while nighttime $R_{Emis\&Trans}$ is most negative at the industrial site (0.76 ppb h^{-1}). Simulations without

OVOCs constraint overestimate OVOCs (42.1~126.5%) and key free radicals (e.g., hydroperoxy radicals (HO$_2$, 5.3%~20.4% and organic peroxy radicals (RO$_2$, 6.6%~35.1%)), leading to a 1.8%~11.9% O$_3$ overestimation. This overestimation causes an underestimation of hydroxyl radicals (OH) (1.8%~20.9%) and atmospheric oxidizing capacity (3.5%~12.5%). These findings emphasize the importance of comprehensive OVOCs measurements to constrain numerical models, especially in regions with dense anthropogenic emissions, to better reproduce atmospheric photochemistry, and to formulate more effective air pollution control strategies.

1. Introduction

Oxygenated volatile organic compounds (OVOCs), contributing 20.1%~73.5% of total volatile organic compounds (VOCs) (Han et al., 2019; Huang et al., 2020; Li et al., 2022a; Liu et al., 2024; Song et al., 2024), are critical components of tropospheric photochemistry (Yang et al., 2014). Photolysis of OVOCs has been proved to be the most significant primary source of RO$_x$ (OH + HO$_2$ + RO$_2$) in Guangzhou, Beijing, and Xi'an in China (Wang et al., 2022c; Yang et al., 2018; Zhang et al., 2021b), and thereby accelerating the recycling of radicals to promote ozone (O$_3$) formation (Qu et al., 2021; Wang et al., 2022c). In addition, previous studies have shown that sufficient free radicals produced by photolysis of OVOCs are the dominated contributors to O$_3$ pollution during winter (Edwards et al., 2014; Emmerson et al., 2005). The study of Li et al. (2021b) indicates that the fast generation of O$_3$ during winter haze in the North China Plain is mainly driven by the photolysis of formaldehyde (HCHO), which leads to a large production of HO$_x$ radical and offsets the radical titration induced by NO$_x$ emissions. In addition, HCHO and other OVOCs dominated the OH loss with VOCs (Goldan et al., 2004), resulting in predominant role in OH reactivity (Ling et al., 2014; Yang et al., 2018). Therefore, OVOCs play a significant role in the atmospheric chemistry.

47   OVOCs have complex and diverse sources, including primary emissions from anthropogenic,

48   e.g., vehicle exhausts (Gentner et al., 2013; Legreid et al., 2007; Wang et al., 2022b), volatile

49   chemical product use (Ou et al., 2015), industries (Wang et al., 2023), biomass combustion (Gilman

50   et al., 2015; Karl et al., 2007; Li et al., 2014a; Yokelson et al., 2007), and biogenic sources (Ou et

51   al., 2015; Rieksta et al., 2023). They are also formed secondarily through photochemical reactions

52   (Huang et al., 2020; Song et al., 2024; Xia et al., 2021). Mo et al. (2016) estimated that OVOCs

53   from heavy-duty diesel vehicle emissions accounted for 53.8% of total VOCs in China, and OVOCs

54   account for 12.4%~46.3% of VOCs emission from biomass and residential coal combustion, which

55   demonstrates the importance of combustion-related sources of OVOCs. In addition, measurement

56   of VOCs fluxes based on the airborne eddy covariance technique showed that urban emission

57   sources comprise a surprisingly large proportion of OVOCs (29%~56%) (Karl et al., 2018;

58   Pfannerstill et al., 2023). Due to the high share of OVOCs in VOCs, previous studies have reported

59   that OVOCs could contributed 38%~60% of ozone formation potential (OFP) (Liu et al., 2024; Mo

60   et al., 2022; Wang et al., 2022a, 2024). The loss of OVOCs occurs through photolysis, reactions

61   with oxidants (e.g., OH, NO_3, and O_3), dilution mixing and deposition (Atkinson, 2000; Atkinson

62   and Arey, 2003). Moreover, air mass transport also can significantly affect the mixing ratio of

63   OVOCs.

64   Chemical transport models (CTMs) have been widely used for the study of formation

65   mechanism of OVOCs and their influence on air quality (Chen et al., 2022; de Gouw et al., 2018;

66   Luecken et al., 2012; Steiner et al., 2008; Yang et al., 2023). However, due the deviation of the

67   meteorological field, uncertainty of the emission inventory (Li et al., 2019; McDonald et al., 2018;

68   Shen et al., 2019), defects of lumped chemical mechanism (Li et al., 2014b; Sarwar et al., 2008;

Stockwell et al., 1997a; Venecek et al., 2018), there is a large uncertainty in the OVOCs simulated

by CTMs, which in turn leads to large deviations in the simulated atmospheric photochemistry. The

observation-based model (OBM) can avoid these biases to a certain extent by constraining

meteorological parameters and chemical species, and leveraging detailed chemical mechanism (e.g.,

Master chemical mechanism, MCM). Nevertheless, due to the limited observations of OVOCs (e.g.,

Pfannerstill et al., 2023), many existing studies use OBM without the observed OVOCs data, or

only with limited inputs for certain OVOCs species (formaldehyde, acetaldehyde, acetone), which

can greatly bias the assessment of O_3 generation mechanism, free radical chemistry, and atmospheric

oxidation. Wang et al. (2022a) showed that the box model without the constraint of OVOCs

underestimates the OVOCs concentrations, which in turn lead to the underestimation of RO_x and O_3

formation. Thus, it is meaningful to couple OVOCs observation with OBM to investigate how

OVOCs affect radical chemistry, atmospheric oxidization capability, and O_3 formation mechanism.

Zibo, a typical industrial cluster city in China, has been suffering from O_3 pollution for years

(Li et al., 2021a; Qin et al., 2023). However, comprehensive studies involving the observation of

VOCs, particularly OVOCs such as HCHO, are rare. Qin et al. (2023) used observations of 98 VOCs

(without HCHO) in Zibo to constrain OBM, but the absence of HCHO in their simulation could

result in underestimation RO_x, thus disturbing the investigation of OH budget (Fuchs et al., 2017;

Guo et al., 2021; Ling et al., 2014; Qu et al., 2021; Tan et al., 2017). This study hypothesizes that

incorporating observational constraints on OVOCs significantly influences the OBM simulations.

To evaluate this, a 5-day field campaign was conducted across five representative sites in Zibo.

Concentrations of 74 VOC species, including 29 alkanes, 16 aromatics, 9 alkenes, 18 OVOCs,

acetylene and isoprene, are obtained. The contributions of secondary formation, emissions/transport

91 to OVOCs level are analyzed by the OBM. Additionally, the impact of OVOCs on radical chemistry,

92 atmospheric oxidation capability, and consequently O_3 production are quantified.

2. Methodology

2.1 Sampling sites and measurements

95   To capture a typical ozone pollution case, the field campaign was conducted from August 8 to

96 August 12, 2021, at five monitoring sites (Zhonglou (ZL), Chengdong (CD), Chengqu (CQ),

97 Tianzhen (TZ), and Xindian (XD)) in Zibo (Figure 1, Table S1). Among the five sites, ZL site

98 (117°54'E, 36°39'N) is an urban site, which is located in the central area of Zibo, and is mainly

99 surrounded by residential areas and factory buildings. According to the prevailing wind direction

100 (northeast, Figure S1 (a)), CQ (118°60'E, 36°57'N) site is an upwind site, while CD (117°53'E,

101 36°31'N) is a downwind site. CD is located on a hillside in the southern part of Zibo, with a small

102 number of ceramic and refractory enterprises factories nearby. TZ (117°48'E, 37°10'N) is close to

103 Shengli Oil field on the west, and is surrounded by farmland. This site is regarded as a suburban site

104 and is affected by residential emissions in the north of Zibo, as well as nearby oil production

105 operations. XD (118°19'E, 36°48'N) is close to a chemical industrial park and serves as an industrial

106 site. More detailed information about these sites can be found in Table S1.

107   Site-scale wind patterns can affect the levels and spatial distribution of OVOCs and PAMS

108 (target VOC species from the Photochemical Assessment Monitoring Stations, including include 29

109 alkanes, 16 aromatics, 9 alkenes, isoprene, and acetylene) across sites. Urban (ZL) and downwind

110 (CD) sites are impacted by OVOC pollution from northeasterly (NNE, NE, ENE) winds, while the

111 upwind (CQ) site experiences higher OVOC and VOCs pollution under both northeasterly and

112 northwesterly (WNW, NW, NNW) winds (Figure S2 (a, b)). Suburban (TZ) and industrial (XD)

113   sites exhibited higher OVOC and VOCs levels under southeasterly (SE) and southwesterly (WSW)

114   winds, respectively, likely due to upwind emissions from nearby industrial sources. WS between 1

115   and 2 m s^{-1} were most common (40.4%) during the observation period. At suburban (TZ) and

116   industrial (XD) sites, OVOC and VOCs levels were lower at low wind speeds (WS < 2 m s^{-1}) than

117   that at higher wind speeds, reflecting the influence of local emissions (Figure S2(c, d)). In contrast,

118   at downwind (CD) site, higher OVOC and VOCs levels were observed at WS > 2 m s^{-1}, indicating

119   the impact of regional transport. At the urban (ZL) site, higher WS are associated with lower VOCs

120   levels and higher OVOC levels, indicating the influence of aging air masses transported from

121   upwind regions.

122
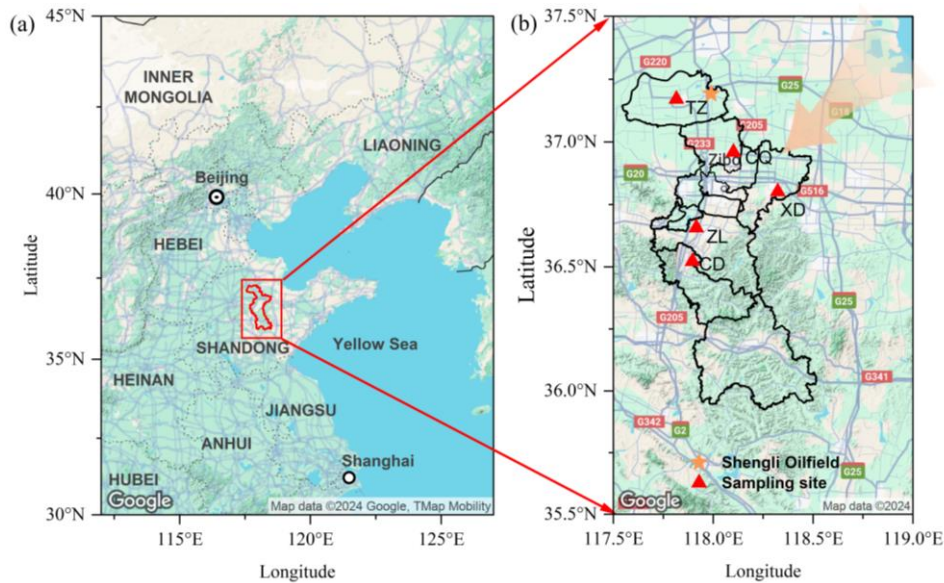
123 **Figure 1. (a) Map of the North China Plain and (b) map of Zibo with locations of VOCs monitoring stations**

124 **(red triangles), and Shengli Oil field (yellow star), and prevailing wind direction (orange arrow).**

125   During the campaign, two online gas chromatography-flame ionization detector (GC-FID,

126   Thermo Scientific GC5900) systems were deployed at suburban (TZ) and upwind (CQ) stations,

127   and three online gas chromatography-flame ionization detector (GC-FID, Syntech Spectras GC

128   955–615/815) systems were deployed at downwind (CD), industrial (XD) and urban (ZL) stations,

129   respectively. A mixture of 56 PAMS target species (Spectra Gases Inc., USA, Table S2) was used

for the calibration of the GC-FID system. Each VOC analyzer provided measurements with a 1-hour temporal resolution. More detailed descriptions of these instruments can be found in previous studies (Li et al., 2023; Wang et al., 2014; Yang et al., 2022; Zheng et al., 2023). Overall, the detection limits for most VOC species are below 0.1 ppb. Additionally, 18 oxygenated VOCs species were collected by 2,4-dinitrophenylhydrazine (DNPH) sorbent tubes in conjunction with an automated sampler for a period of 1 or 3 hour per sample. A 47 mm quartz filter membrane is attached to the front of the sampling tube to filter particulate matter. An ozone scrubber (silica gel column tubing coated with potassium iodide) was placed at the front of the air inlet to avoid ozone interference. OVOCs were derivatized in cartridges to hydrazones during sampling. The cartridges were eluted with 3 mL of acetonitrile and stored at 0-4 °C immediately. Then the eluants were analyzed using an Agilent HPLC, equipped with ultraviolet absorption detector (UVD), quadruple pump, and Agilent TM C18 reversed column (250 mm×4.6 mm, 5.0 μm). A gradient elution was used, and the mobile phase was mixing of acetonitrile, tetrahydrofuran and water. The analysis was carried out using a ternary gradient elution program at a flow rate of 1.2 mL/min, with detection wavelength of 360 nm, and sample volume of 10 μL at a column temperature of 45 °C. More details about OVOC samplings and analysis can be found in Peng et al. (2023). The lower limit of detection for OVOCs were <0.1 ppb (Peng et al., 2023). A total of 271 valid OVOCs samples were collected during the campaign. At the industrial (XD) and suburban (TZ) stations, 8 samples were collected per day at 3-hour intervals. At the urban (ZL), upwind (CQ) and downwind (CD) stations, 10 samples were collected per day, with 7 samples collected at 1-hour intervals during 7:00-21:00 LT, and 3 samples collected at 3-hour intervals during the night (1:00-6:00 and 22:00-1:00[+1] LT), and totaling 59 valid samples per station. Finally, a total of 74 VOCs (56 PAMS and 18 OVOCs) were

152   combined to conduct data analysis in this study (Table S2). Conventional gas phase pollutants (e.g.,

153   O_3, CO, and NO_x (NO and NO_2)) were measured using commercial online analyzers (Thermo

154   Scientific 49i, 48i, and 42i, USA) at each site. NO_x was measured by NO chemiluminescence and

155   chemical conversion with a molybdenum convertor, which is known to be interfered by NO_z species

156   (Tan et al., 2017, 2019a). Meteorological parameters, including temperature (T), relative humidity

157   (RH), wind speed (WS), wind direction (WD), and ambient pressure (P) were obtained

158   synchronously by Chinese ground-based meteorological stations (Boshan, Huantai, Gaoqing, Linzi,

159   and Zichuan sites) (http://data.cma.cn/, last access: March 26, 2024).

160   **2.2 Observation-based model**

161   A box model (F0AM) coupled with the Master Chemical Mechanism (MCM) v3.3.1 was

162   utilized to simulate the in situ atmospheric chemical process at these 5 sites (Jenkin et al., 2015;

163   Wolfe et al., 2016). The MCMv3.3.1, as a nearly explicit mechanism with more than 5800 species

164   and 17000 reactions, provides a more detailed gas chemistry than other lumped mechanisms, such

165   as the Carbon Bond Mechanism (CB) (Yarwood et al., 2005, 2010), Regional Atmospheric

166   Chemistry Mechanism (RACM) (Goliff et al., 2013; Stockwell et al., 1997b), and SAPRC (Carter,

167   1990, 2010b; Carter and Heo, 2013). The box model calculations were constrained by

168   comprehensive measurements of trace gases (NO, NO_2, CO, and SO_2) and 45 speciated VOCs,

169   encompassing 20 alkanes, 9 alkenes, 14 aromatics, 15 OVOCs, isoprene and acetylene, as well as

170   meteorological parameters (T, RH and P). To address potential NO_2 measurement artifacts, several

171   adjustments were implemented. Considering that PKU-Mo as a catalytic converter for NO_2

172   measurement can cause interferences from other nitrogen–oxygen compounds (e.g., PAN, HNO_3),

173   potentially overestimating NO_2 by 30%~50% (Kim et al., 2015; Tan et al., 2017, 2019a; Xu et al.,

2013). In this study, the observed NO_2 mixing ratio ($[NO_2]_{obs}$) at the 5 sites were reduced by 30%~40% (40% for ZL and CQ, 30% for CD, TZ and XD) to compensate for catalytic converter interferences (Xu et al., 2013). Additionally, strong anthropogenic emissions (e.g., vehicle emissions) near the sites may prevent the model from reaching steady state, leading to positive deviations (Li et al., 2014c). Therefore, NO steady-state approximations ($[NO]_{ss}$), calculated according to the equations proposed by Del Negro et al. (1999) (Equation S1), was used to constrain the simulated NO. The uncertainties derived from the NO_x settings are shown in Table S3 and analyzed in Section 3.4. HONO was fixed to 2% of the corrected NO_2 mixing ratio ($[NO_2]_{cor}$) (Elshorbany et al., 2012; Tan et al., 2019a), and the corresponding uncertainty is summarized in Section 3.4. In addition, boundary layer height (BLH), and surface net solar radiation (SSR) were obtained from the fifth generation of the European Centre for Medium-Range Weather Forecasts (ECMWF) reanalysis for the global climate and weather (https://cds.climate.copernicus.eu, last access: March 1, 2024). The photolysis frequency correction factor (Jcorr) of the model input was adjusted by SSR. BLH was also included in the model to control the deposition process (Xuan et al., 2023; Zhu et al., 2020).

The model ran with continuous time series profile for the campaign period (August 8-12) with 1-hour time-step. A sensitivity analysis was performed for the time-step and the results are summarized in Section 3.4. Each simulation started with 10-days spin up to reach steady state condition. Missing observation data were filled with linear interpolation, and the mixing ratios of OVOCs were also linearly interpolated to 1-hour resolution for modeling. An artificial loss process corresponding to an atmospheric lifetime of 24 h or a first-order dilution rate (kdil) of $1/86400$ s^{-1} was introduced for all simulated species, including secondary species and radicals, to approximately simulate dry deposition and other losses (Lou et al., 2010; Tan et al., 2018b; Wang et al., 2022c).

196   The model cases that run with the above settings with 15 constrained OVOCs species are called the

197   Base scenario. To investigate the impacts of constrains of OVOCs on atmospheric chemistry, the

198   Free scenario was conducted, with all the setting of the Base scenario except for the OVOCs

199   constraint.

2.3 Budgets of OVOCs and O₃

201   At a given site, variations in OVOCs mixing ratios are mainly influenced by in-situ

202   photochemical production and chemical loss, emissions, regional transport, and deposition (Tan et

203   al., 2018a; Xue et al., 2014a; Zhang et al., 2021). The change rate of observed OVOCs (R_{Meas}) is

204   calculated by Equation (1). The in-situ photochemical production of OVOC ($R_{ChemProd}$) is mainly

205   caused by the oxidation of VOCs, while their in-situ chemical loss ($R_{ChemLoss}$) includes photolysis

206   and reactions with oxidants (OH, NO₃, and O₃) (https://mcm.york.ac.uk/MCM/, last access: 13 Jan

207   2025) (Atkinson, 2000; Atkinson and Arey, 2003; Jenkin et al., 2015; Saunders et al., 2003). The in-

208   situ net OVOCs chemical production ($R_{NetProd}$) (Equation (2)) and their removal by deposition (R_{Dep})

209   are calculated hourly according to the OBM simulation. The OBM primarily accounts for

210   atmospheric photochemical reactions, and deposition within the boundary layer. However, previous

211   studies have reported that the OBM lacks an explicit representation of transport processes and

212   emissions (Wolfe et al., 2016; Zhang et al., 2021), making it challenging to disentangle their

213   respective contributions. Therefore, emissions and transport are combined to a single term

214   ($R_{Emis\&Trans}$) to represent their contributions collectively. If the $R_{Emis\&Trans}$ is positive, it is considered

215   a net import of emissions/transport, whereas a negative suggests a net export. The emissions and

216   regional transport of OVOCs ($R_{Emis\&Trans}$) are computed as Equation (3).

$$R_{Meas} = \sum_i \frac{d([OVOC]_i)}{dt} \tag{1}$$

$$R_{NetProd} = \sum_i (R_{ChemProd,i} - R_{ChemLoss,i}) \tag{2}$$

$$R_{Emis\&Trans} = (R_{Meas} - R_{NetProd} - \sum_i R_{Dep,i}) \tag{3}$$

217   where $[OVOC]_i$ is the mixing ratios of OVOC species i constrained in OBM, 15 in total (Table S2).

218   dt is the time-step of modeling, d$[OVOC]_i$ refer to the change in mixing ratio of OVOC species i.

219   Considering the oxidation of NO to NO_2 by peroxyl radicals, the total oxidant ($O_x =O_3 + NO_2$)

220   is generally used to characterize the chemical budget of O_3 (Kanaya et al., 2009; Xue et al., 2014b).

221   The total chemical production of O_x through oxidations of NO by HO_2 and RO_2 radicals (Tan et al.,

222   2018b), is defined as the production of O_3 (P(O_3)), which is calculated according to Equation (4):

$$P(O_3) = k_{HO2+NO}[HO_2][NO] + \sum k_{RO2,j+NO}[RO_2]_j[NO] \tag{4}$$

223   The chemical loss rate (L(O_3)) of O_3 is equal to the sum of loss rates of O_3 and NO_2, including

224   O_3 photolysis, reactions of O_3 with OH, HO_2 and alkenes, as well as reactions of NO_2 with OH and

225   RO_2, as well as the reaction of NO_3 with unsaturated VOCs (Chen et al., 2020; Liu et al., 2022; Xue

226   et al., 2016, 2014b).

$$
\begin{aligned}
L(O_3) = {} & k_{O1D+H2O}[O1D][H_2O] + k_{O3+OH}[O_3][OH] \\
& + k_{O3+HO2}[O_3][HO_2] + k_{O3+alkenes}[O_3][alkenes] \\
& + k_{NO2+OH}[NO_2][OH] \\
& + \sum k_{NO2+RO2,j}[NO_2][RO_2]_j \\
& + \sum k_{NO3+VOC,i}[NO_3][VOC]_i
\end{aligned}
\tag{5}
$$

227   The concentrations of radicals and intermediates are derived from the outputs of the OBM. The

228   k values in Equations (4) and (5) rate constants of the corresponding reactions, which can be found

229   from https://mcm.york.ac.uk/MCM/ (last access: 13 Jan 2025) or the study by Liu et al. (2022). The

230   subscript 'j' in Equation (4) and (5) denotes individual RO_2 species. The subscript 'i' in Equation

(5) represents individual VOC species. The net O_3 production rate can be obtained from the difference between P (O_3) and L(O_3).

2.4 Evaluation of ozone formation potential and atmospheric oxidation capacity

Different VOC species vary in their capability to form ozone, and their potential to produce O_3 can be evaluated by the maximum incremental reactivity (MIR) (Carter, 2010a). The ozone formation potential (OFP) calculated for each VOC species represents its maximum contribution to ozone production (Bufalini and Dodge, 1983). The OFP of VOCs is calculated as follows:

$$OFP_i = [VOC]_i \times MIR_i \tag{6}$$

where OFP_i is the OFP of VOC species i ($\mu g\ m^{-3}$), $[VOC]_i$ is the atmospheric concentration of VOC species i ($\mu g\ m^{-3}$), MIR_i is the maximum incremental reactivity coefficient of the VOC species i (g O_3/g VOCs) (Table S2) from Carter, 2010a.

Atmospheric oxidation capacity (AOC) is the core driving force of complex air pollution, influencing the removal rate of trace gases and the production rates of secondary pollutants (Liu et al., 2021). AOC is calculated based on the sum of oxidation rates of oxidants (OH, O_3, and NO_3) with primary pollutants (VOCs, CO, and CH_4) (Elshorbany et al., 2009; Geyer et al., 2001; Yang et al., 2022b). The formula is as follows:

$$AOC = \sum_i k_{Yi}[Y_i][X] \tag{7}$$

where Y_i represents primary VOCs (excluding OVOCs), CO and CH_4, X represents oxidants (OH, O_3 and NO_3) and k_{Yi} is the bimolecular rate constant for the reaction of Y_i with X. Atmospheric oxidation capacity determines the rate of Y_i removal.

3. Results and discussion

3.1 Meteorological and chemical conditions

251   The field campaign is characterized by consistent hot and sunny conditions, with the average

252   daily maximum temperature and SSR of 32.2±1.4 °C (peak at 34.1 °C) and $2.1\pm0.4\times10^6$ J m^{-2}

253   (Figure 2, Figure S2 (a)), respectively, which favors the photochemical formation of O_3. A typical

254   O_3 episode was observed, with an average maximum daily 8-hour average O_3 (MDA8-O_3) of 89.8

255   ppb in Zibo city. According to the Chinese National Ambient Air Quality Standard Grade II (about

256   93.3 ppb for 1-hour average, or 74.7 ppb for MDA8-O_3), there are four O_3 pollution days (August

257   8 to 11) during the campaign. The average mixing ratios of SO_2, NO_2, NO, and CO in Zibo are

258   2.8±1.6, 12.0±6.9, 2.8±4.8, and 897±670 ppb, respectively (Figure 2, Figure S3 (b)). The mean

259   VOCs mixing ratio in this study is 44.6±20.9 ppb, which is overall higher than that in Beijing

260   (18.3±8.9 ppb) from July 23 to August 31 in 2016 (Wu et al., 2023), Rizhao (9.83 ppb) in summer

261   in 2022 (Zhang et al., 2023), and Xi'an (29.1± 8.4 ppb) from June 20 to July 2019 (Song et al.,

262   2021). Compared with the median VOC levels (~32 ppb) in other cities in China (Figure 3, Table

263   S4), VOC levels in Zibo is in the upper-middle range. Previous studies have demonstrated that

264   industrial processes account for approximately 49% of total VOC emissions in Shandong Province

265   (Jiang et al., 2020; Li et al., 2017; Ren, 2011; Zheng et al., 2021). This indicates strong

266   anthropogenic VOCs emission in Zibo. Notably, VOC emission intensity in Zibo was among the

267   highest in Shandong Province, with values > 90 t km^{-2} y^{-1}, even >108 t km^{-2} y^{-1}in some areas in

268   2016 (Jiang et al., 2020; Zhou et al., 2021). In terms of the VOCs groups (Figure 5 (c), Figure S4

269   (a)), alkanes and OVOCs were the two predominant groups at each site, accounting for 33.3~51.5%

270   and 30.0~37.8% to the total VOCs, respectively, followed by aromatics (3.8~16.5%) and alkenes

271   (5.0~13.8%). In addition, the difference between peak and valley NO_2 mixing ratios was 14.4±3.2

272   ppb, indicating that substantial NO_x was converted to O_3.
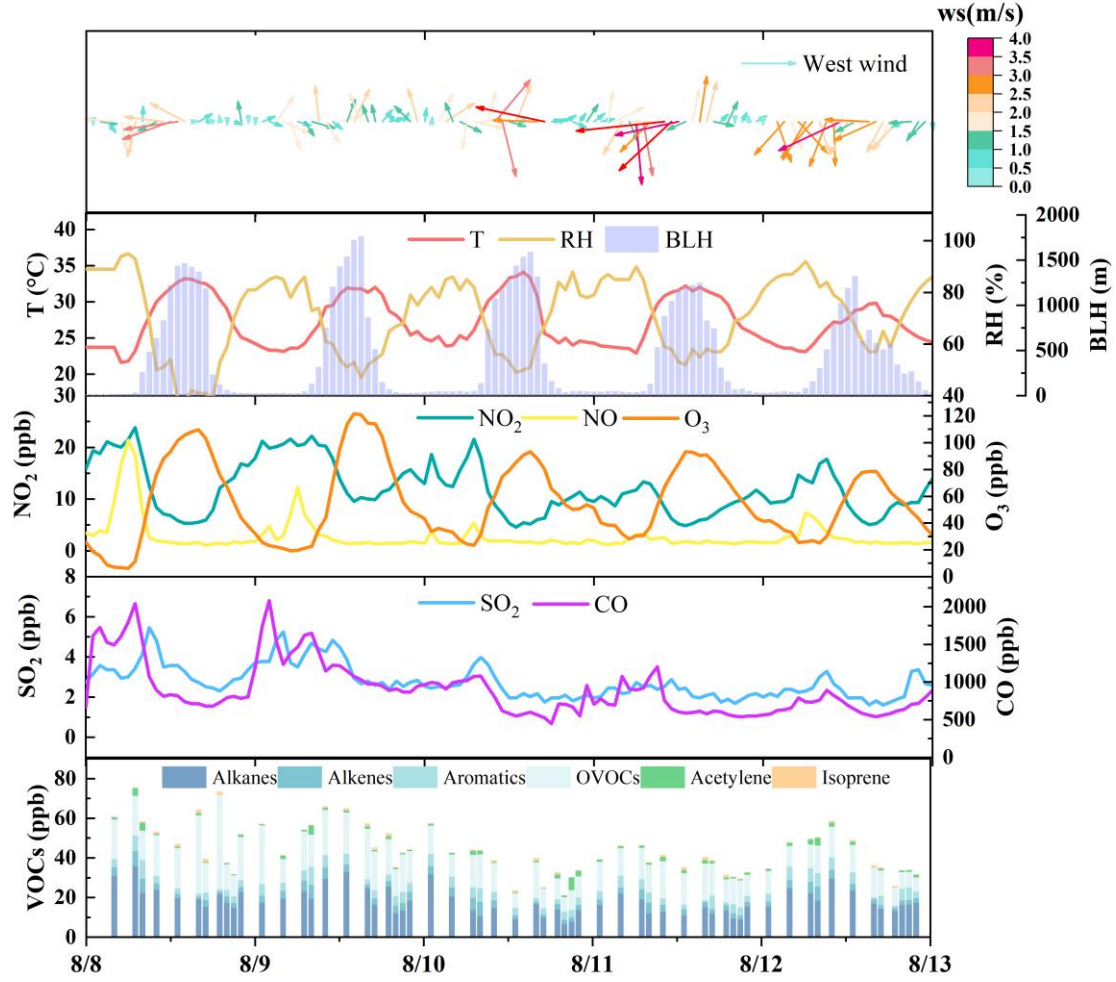
273
274 **Figure 2. Time profiles of pollutant mixing ratios and meteorological parameters in Zibo from August 8 to**
275 **12, 2021. The meteorological data were from ZL, the central site of Zibo, and the pollutants data were the**
276 **average of the five sites. The hourly PAMS (including alkanes, alkenes, aromatics, acetylene, and isoprene)**
277 **data were aligned with the 1/3-hour sampling intervals of the OVOCs data to ensure comparability between**
278 **the two datasets.**

279
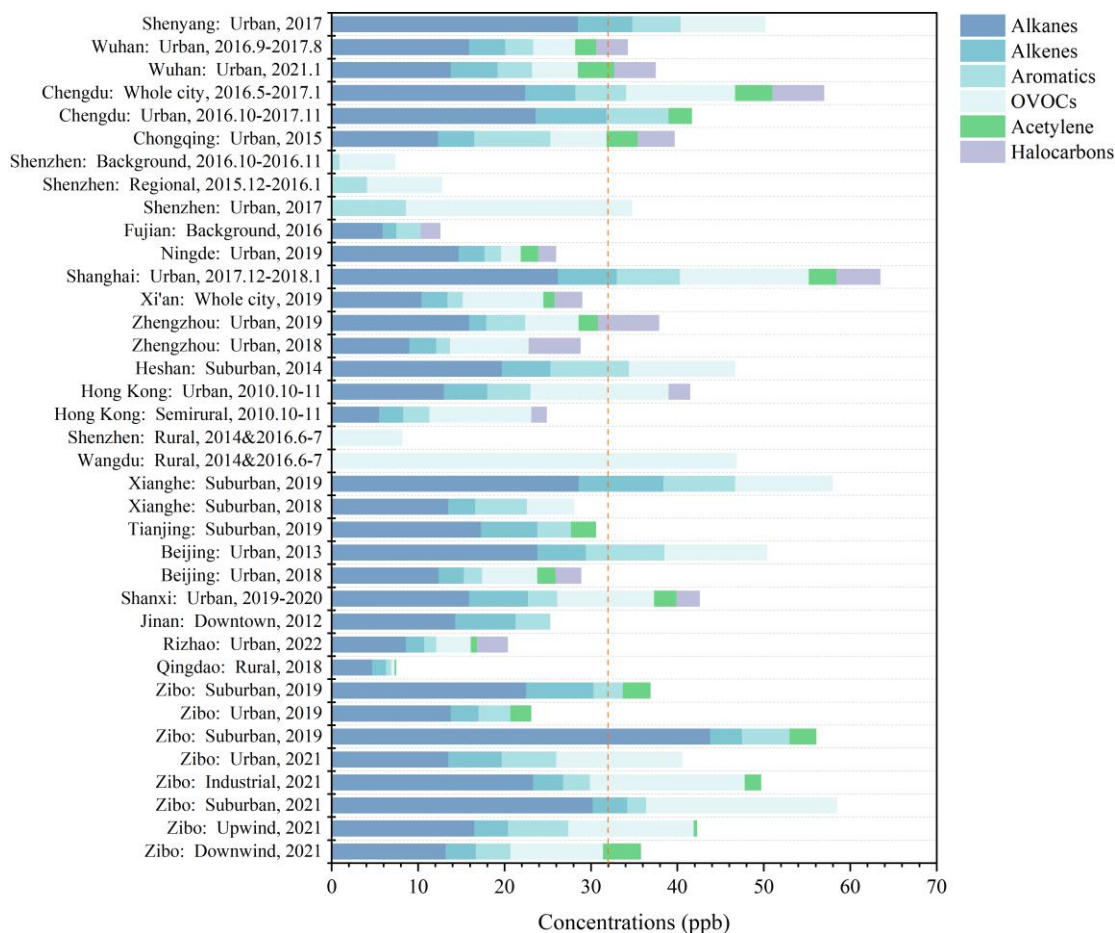
Figure 3. Comparison of VOC mixing ratios and compositions in this study with former studies based on Table S4. The red dash line represents the median levels (~32 ppb) of VOCs。

282
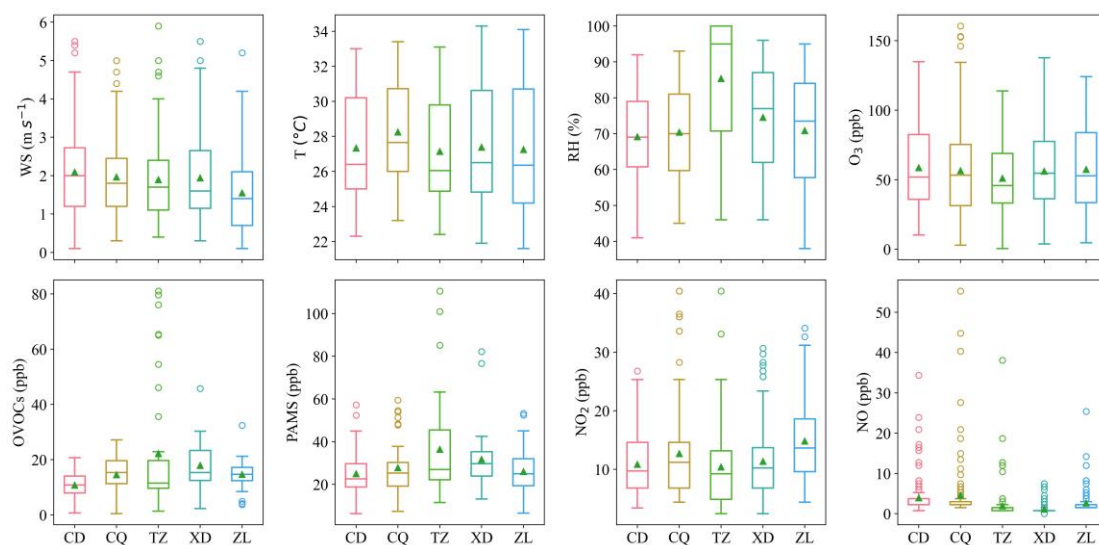
Figure 4. Distribution of O₃ and its precursors (OVOCs, PAMS, NO₂, and NO) and meteorological parameters (WS, T, and RH) at five sites, with the green triangle being the mean value and the horizontal line in the box being the median.

Across the five sites, the O₃ mixing ratios are comparable across all the sites (Table S6, Table

287 S11) (p > 0.05). However, TVOCs at suburban site (TZ, 58.5±35.0 ppb) is the highest (Figure 5 (c),

288 Figure S4 (b)), which is attributed to oil refineries near this site. The downwind site (CD) has slightly

289 lower NO_2 level (10.8±5.1 ppb) and lower TVOCs mixing ratios (35.7±12.5 ppb) than urban site

290 (ZL, 14.8±6.5 and 40.6±10.3 ppb, respectively) and upwind site (CQ, 12.7±8.1 and 42.3±15.4 ppb,

291 respectively), and has higher O_3 mixing ratio (58.6±30.0 ppb) than CQ and ZL station. This may be

292 attributed to the sequential transport of O_3 and its precursors from the upwind station (CQ) to urban

293 station (ZL), and subsequently to the downwind station (CQ), driven by the dominant northeasterly

294 winds (Figure 1 (b), Figure S1).

295   According to the time series of individual pollutant (Figure S3 (b)), CQ showed obvious peak

296 mixing ratios of O_3, NO_2, NO and CO than the other sites during August 8-9, with stagnant

297 conditions (WS < 2 m s^{-1}), indicating stronger emissions from combustion sources and possibly fast

298 photochemical process near CQ. In addition, XD showed high mixing ratios of CO during August

299 8-9, and high daytime TVOCs levels on August 9 (9:00-14:00 LT, 90~110 ppb). Given CO's

300 relatively inert nature and the absence of similar CO peaks at the other four sites, the abnormal CO

301 peak at XD is related to strong emissions from nearby factories in the industrial park. TZ showed

302 distinct morning and evening peaks of TVOCs at 6:00 LT (163.0 ppb) and 21:00 LT (120.0 ppb) on

303 August 8, and a night peak at 1:00 LT on August 10 (130.3 ppb), which were attributed to emissions

304 from the neighboring oil field operations. From August 10 to 12, as wind speeds increased,

305 pollutants levels at all sites decreased to similar levels. Overall, local anthropogenic emissions in

306 Zibo were more prominent under weak wind conditions.

307   To compare the secondary O_3 formation in each site, the ozone formation potential (OFP) of

308 each VOCs is calculated (Equation (6)). The mean OFP in Zibo during the observation is

410.4±197.2 µg m^{-3}, with OVOCs accounting for the largest proportion (31.5%~55.9%), followed by aromatics (10.2%~41.2%). Alkanes (10.3%–24.6%) and alkenes (11.4%~23.1%) make comparable proportions, while BVOCs accounted for only 2.1%~7.6% of the total OFP (Figure 5 (b)). The one-way analysis of variance (ANOVA) results ($p < 0.05$) indicate significant differences (Armstrong et al., 2000) in VOC subclass contribution to OFP across the 5 sites. Alkanes and aromatics show larger F-values (Table S11), reflecting greater variations in the contributions to OFP across the 5 sites, whereas OVOC and BVOC (isoprene) exhibited lower variability. Post-hoc Tukey honestly significant difference (HSD) tests were performed followed ANOVA to further identify specific significant differences in VOC subcategories between sites (Figure S14). The OFP of TVOCs is generally similar across stations, except for the downwind station (CD). The upwind station (CQ, 464.2±162.3 µg m^{-3}) has the highest OFP, followed by the suburban site (TZ, 456.3±295.3 µg m^{-3}), the urban site (ZL, 441.1±174.5 µg m^{-3}), the industrial site (XD, 422.9±166.9 µg m^{-3}), and the downwind site (CD, 279.4±101.2 µg m^{-3}) (Table S5). Differences in OFP levels of aromatics and alkanes at downwind station (CD), suburban station (TZ) and industrial station (XD) are minimal (Figure S14 (b, c)). However, significant differences in OFP contributed by OVOC at downwind station (CD) compared to suburban station (TZ) and industrial station (XD) are attributed to OVOC emission sources, regional transport and secondary formation (Figure S14 (a)). Apart from CQ, OVOCs are the dominant contributors to OFP at each site, especially TZ and XD, with mean OFP of 254.9±276.1 µg m^{-3} (55.9%) and 194.7±101.0 µg m^{-3} (46.0%) from OVOCs, respectively. This indicates the key role of OVOCs in the formation of O$_3$ at our observational sites. Among OVOC species, HCHO is the dominant contributor to OFP across the five sites (56.6~202.0 µg m^{-3}). This is consistent with previous studies (Duan et al., 2008; Huang et al., 2020; Zhou et al., 2024).

331 The top four OVOC species are formaldehyde, acetaldehyde, propionaldehyde, and butyraldehyde,

332 which cumulatively contributed 91%~95% of the OFP from OVOCs (Table S5). Additionally, the

333 variety of VOCs sources, meteorological condition, and photochemical condition in each site lead

334 to differences in key species of OFP at each site. At the suburban site (TZ), isoprene (34.9 μg m^{-3})

335 ranks 2nd in terms of OFP after formaldehyde (202.0 μg m^{-3}), indicating a high impact of biogenic

336 emissions (Mo et al., 2018; Sindelarova et al., 2014). At the industrial site (XD), the contribution of

337 isopentane, marker of oil and gas emissions, to OFP is more prominent (as high as 66.2 μg m^{-3}) than

338 other sites. OFP of highly reactive aromatic hydrocarbon species, such as m/p- xylene (53.8 μg m^{-}

339 ^{3}) and o-xylene (23.6 μg m^{-3}) are predominant at upwind site (CQ), indicating outstanding

340 contribution of solvent-using sources. OFP contributed by alkenes is the highest at urban site

341 (101.8±56.8 μg m^{-3}) (Figure 5 (a)), with ethylene and propylene being the most key species, which

342 is consistent with the dense vehicle emission near this site.

343
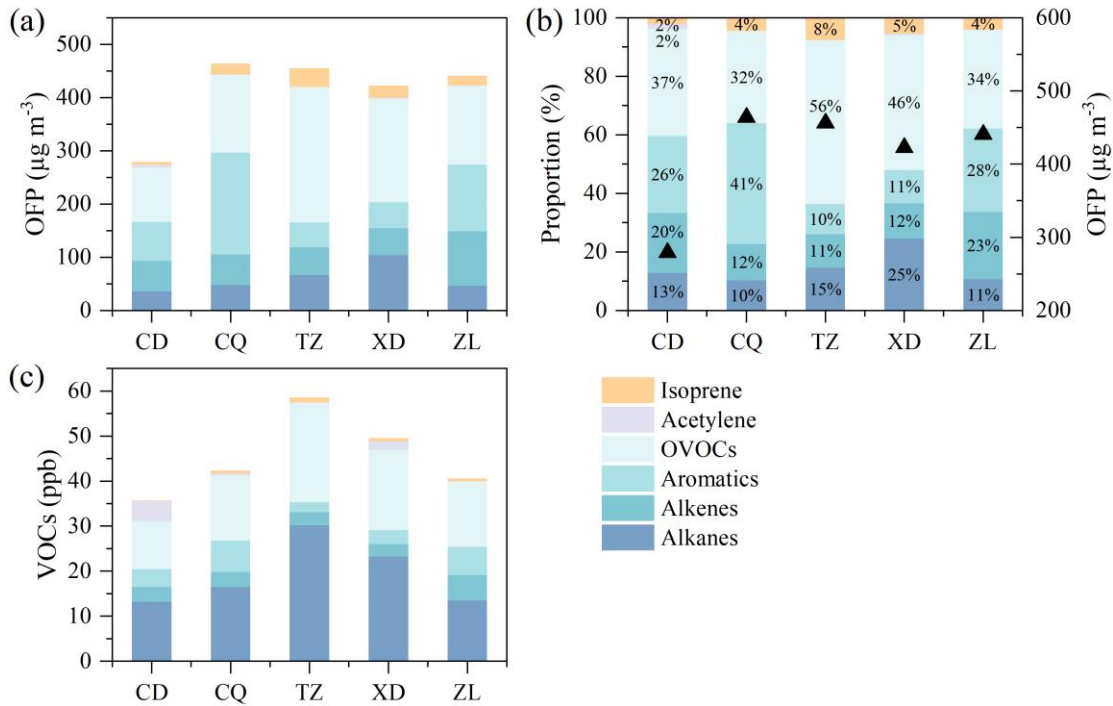
344 **Figure 5. (a) Ozone formation potential (OFP) and (b) proportions of OFP contributed by VOC subgroups,**
345 **along with (c) mixing ratios of VOC subgroups at five sites.**

3.2 Contribution of chemical generation, emissions/transport to OVOCs

OBM simulation results were used to analyze the contributions of chemical processes, and emissions/transport to OVOCs. Overall, the modeled O_3 in the Base scenario exhibited good model performance at the five sites, with R values exceeding 0.85 and IOA values greater than 0.80 (Table S7). These metrics indicate a high level of agreement between observed and modeled data, comparable to results reported in previous studies (Qin et al., 2023; Zheng et al., 2023). The contributions of $R_{NetProd}$ predominantly occur during the daytime (Figure 6). The maximum average daytime $R_{NetProd}$ of OVOCs was observed at ZL (5.9±3.5 ppb h^{-1}), followed by CQ (4.11±11.9 ppb h^{-1}), XD (3.6±2.4 ppb h^{-1}), CD (3.5±2.0 ppb h^{-1}) and TZ (1.9±3.6 ppb h^{-1}) sites. This suggests that abundant reactive VOCs emissions at urban areas as well as in the industrial areas could lead to faster generation of OVOCs. Generally, the $R_{NetProd}$ varied with a single peak due to photochemical formation and export transport, with the maximum value at 12:00-14:00 LT. The mean peak of $R_{NetProd}$ at ZL was 8.8 ppb h^{-1}, followed by XD (5.6 ppb h^{-1}), CQ (5.5 ppb h^{-1}), CD (5.1 ppb h^{-1}) and TZ (3.0 ppb h^{-1}). Generally, in the early morning hours (4:00-10:00 LT), positive R_{Meas} at CD, CQ, and XD sites are driven by $R_{Emis\&Tran}$ import. During this period, OVOCs mixing ratios show a significant upward trend, peaking between 8:00 and 10:00 LT.

Overall, OVOCs mixing ratios at CD, CQ, and ZL sites were typically lower at night but higher during the daytime (Figure 6), attributing to strong daytime photochemical generation, especially at around 7:00-10:00 LT. In contrast, TZ and XD showed higher nighttime OVOCs than that at daytime, which is due to stronger emission import during night. In addition, though $R_{NetProd}$ at ZL was the fastest during the daytime, the airmass transport can efficiently export OVOCs to downwind areas, leading to relatively lower OVOCs mixing ratios. While at TZ, $R_{NetProd}$ was the lowest, but the

368   daytime OVOCs was the highest due to the predominant daytime import, especially the

369   southwestward import on August 8 (Figure S5 (f)).
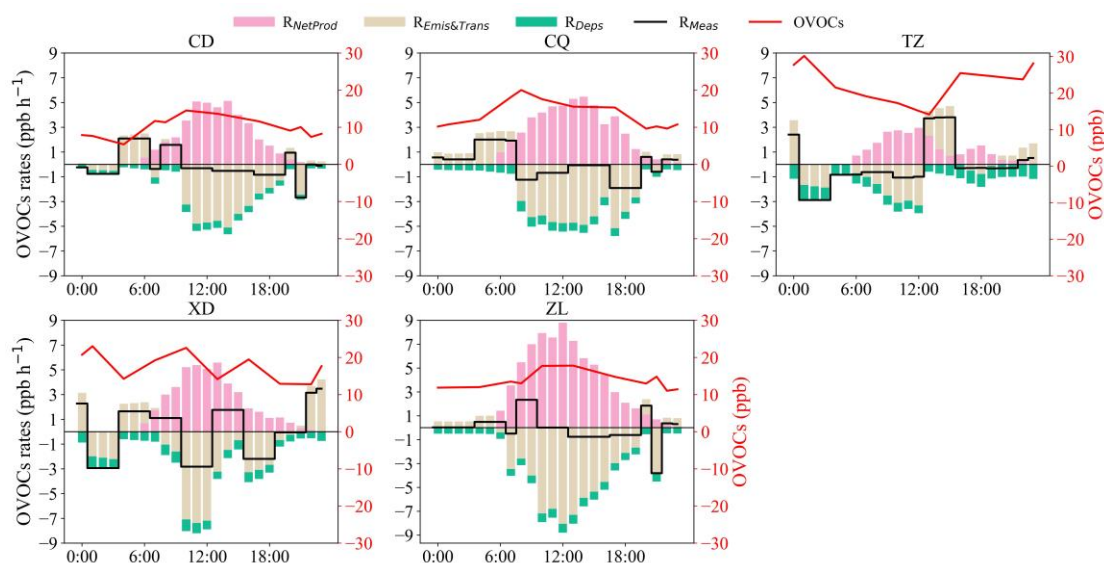
370
371   **Figure 6. Diurnal profiles of OVOCs contributions from local photochemical production (R_NetProd),**

372   **deposition (R_Deps), emission/transport (R_Emis&Trans), and measured OVOCs formation rate (R_Meas) of the five**

373   **sites.**

374   **3.3 Importance of OVOCs observationally constraint in OBM**

375   To investigate the effect of the constrain setting of OVOCs on OBM performance, the

376   simulated OVOC, O_3, radicals in the Free and Base scenarios are compared (Figure 7). It has been

377   shown that the box model, which did not take into account transport (including horizontal and

378   vertical diffusion) and emissions, will result in overestimations of OVOCs, peroxyl radical and PAN

379   (Qu et al., 2021). In this study, OVOCs are overestimated by 42.1%~126.5% in the Free scenario

380   compared with the Base scenario (Figure 7 (a), Figure S6 (c)), especially HCHO (76.3%) and

381   benzaldehyde (737.5%). The daytime RO_x was overestimated by 6.5%~23.3%, with RO_2 and HO_2

382   being overestimated by 6.6%~35.1% and 5.3%~20.4%, respectively, while OH was underestimated

383   by 1.8%~20.9% (Figure 7 (d-f), Figure S7 (b)). As shown in Figure 8 (a), photolysis of OVOCs

384   (include HCHO) is the predominant source of RO_x radicals ($P(RO_x)$) in the daytime, which is

385   consistent with the findings in Beijing (Liu et al., 2012), Shanghai (Zhang et al., 2021a), Hong Kong

386 (Xue et al., 2016), and Mexico (Volkamer et al., 2010). To assess the impact of OVOCs on the

387 simulation of RO_x species (RO_2, HO_2, and OH), the chemical budgets of these species, as influenced

388 by OVOCs, are quantified according to Liu et al. (2012) and Xue et al. (2016) (Figure 8 (b), Figure

389 S8 (a)).

390   In the Free scenario, the daytime net production of RO_x ($P(RO_x)$) was estimated to range from

391 0.03~0.14 ppb h^{-1} across four sites (excluding TZ), indicating an overestimation of RO_x. Notably,

392 the TZ site exhibited negative $P(RO_x)$ values, suggesting the potential existence of unaccounted RO_x

393 sources in this region. The mean daytime $P(RO_x)$ in the Free scenario was calculated as 4.8±2.7 ppb

394 h^{-1}, 18.8% higher than that in the Base scenario (4.0±2.3 ppb h^{-1}). As illustrated in Figure 8 and

395 Figure S8(a), the photolysis of OVOCs (including HCHO) dominants $P(RO_x)$, with a mean rate of

396 2.9±1.9 ppb h^{-1} in the Free scenario, 27.4% higher than that in Base scenario (2.3±1.5 ppb h^{-1}). This

397 substantial increase in OVOCs photolysis consequently amplified the formation of peroxyl radicals

398 (RO_2 and HO_2). Among the production pathways, the photolysis of HCHO demonstrated the most

399 pronounced impact on HO_2 production in the Free scenario (0.1~1.9 ppb h^{-1}), with an increase of

400 7.8%~151.2% (0.1~1.2 ppb h^{-1}) than in the Base scenario (0.5~1.1 ppb h^{-1}) (Figure 8 (b)).

401   The interference of OVOCs on OH is comprehensive. On the one hand, increased OVOCs

402 tends to elevate the generation of HO_2, which can directly or indirectly boost OH generation via the

403 reaction of NO (Figure S9). On the other hand, the higher OVOCs levels can decrease OH via the

404 reaction of OH+OVOCs (Qu et al., 2021; Tan et al., 2019b). In the Free scenario, total OH sources

405 (including H_2O_2+hv, HONO+hv, O_3+hv, and HO_2+NO) is 7.5~12.1 ppb h^{-1}, which is 0.3~1.1 ppb h^{-}

406 ^{1} higher than that in the Base scenario (10.2~11.0 ppb h^{-1}) (Figure S9). Conversely, OH destruction

407 to peroxyl radicals in the Free scenario (7.1~11.8 ppb h^{-1}) is 0.3~2.1 ppb h^{-1} higher than that in Base

408 scenario (6.1~9.7 ppb h⁻¹), leading to a net OH loss of 0.1~0.9 ppb h⁻¹. This underestimation of OH

409 without OVOCs constraint biases atmospheric oxidation capacity (AOC) by 0.1%~10.0%

410 (excluding XD) (Figure S10), affecting the evaluation of VOCs decay via OH oxidation (Li et al.,

411 2022).
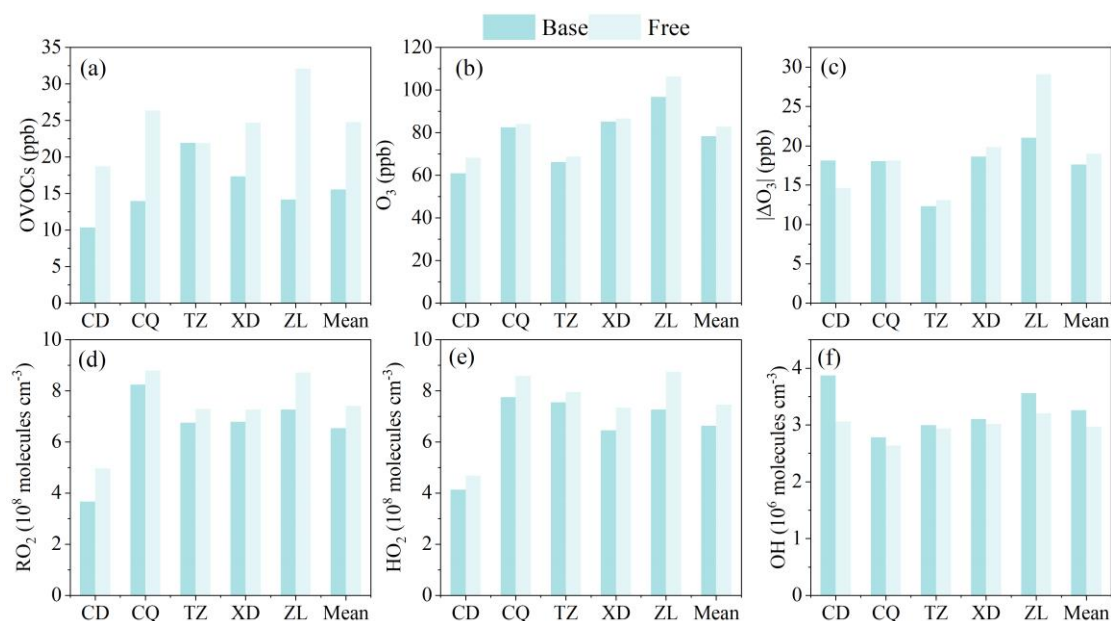
412
413 **Figure 7. Comparison of average (a) OVOC, (b) daytime O₃, (c) daytime |ΔO₃| (the gap between simulated**
414 **and observed daytime (8:00-18:00 LT) O₃ mixing ratios), and ROₓ ((d) RO₂, (e) HO₂, and (f) OH) between**
415 **the Base and Free scenario simulations.**
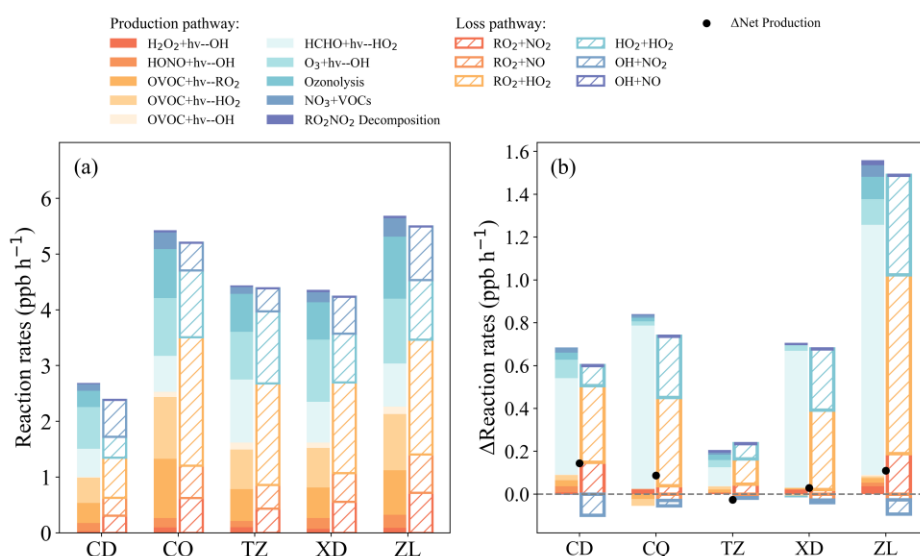
416
417 **Figure 8. (a) Average daytime (8:00-18:00 LT) sources and sinks of ROₓ in Base case and (b) the impact of**
418 **OVOCs observationally constraints on ROₓ budget, calculated by the difference between the Free and Base**
419 **scenarios.**
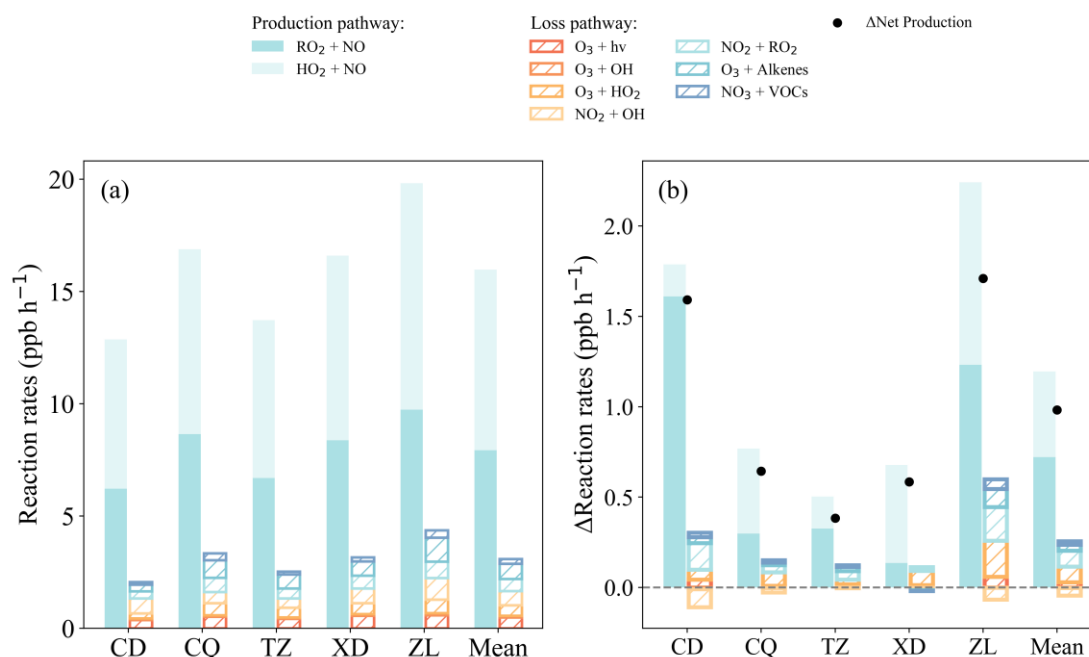
Figure 9. (a) Average daytime (8:00-18:00 LT) O_3 production and loss rates (ppb h^{-1}) in Base scenario and (b) the impact of OVOCs observationally constraints on O_3 budget, calculated by the difference between the Free and Base scenarios.

Overall, the gap between simulated and observed daytime O_3 mixing ratios ($|\Delta O_3|$) in the Free case increased by 7.5% compared to that in the Base scenario. To better understand the influence of OVOCs on O_3 formation, the rates of the main production and sink pathways of O_3 in the Base and Free scenarios are summarized (Figure 9, Figure S8 (b)). Compared to the Base scenario, the diurnal $P(O_3)$ in the Free scenario increases by 3.7%~13.9%, with the reaction rates of RO_2+NO and HO_2+NO increases by 1.6%~25.9% (0.1~1.6 ppb h^{-1}) and 2.5%~10.0% (0.2~1.0 ppb h^{-1}), respectively. This is attributed to the elevated RO_2 and HO_2 radical concentrations simulated without constraints of OVOCs observations (Figure 7 (d-e)). In contrast, the lower simulated concentration of OH radicals in the Free scenario results in a 0.5%~14.8% (0~0.1 ppb h^{-1}) decrease in the $OH+O_3/NO_2$ reaction rate. Although the $L(O_3)$ in the Free scenario is 0.4~1.7 ppb h^{-1} higher than that in the Base scenario, it cannot offset the increase of $P(O_3)$, leading to higher net product of O_3. Thus, no constraints of OVOCs could lead to overestimate peroxyl radicals in the OBM, which in

turn significantly overestimates the deviation of O_3 due to the formation pathway of RO_2/HO_2+NO.

Of course, the impact of OVOCs varies considerably in different emission and functional regions.

The simulated mean daytime O_3 in the Free scenario is 106.3, 86.7, 84.1, 68.8, and 68.2 ppb h^{-1} at

ZL, XD, CQ, TZ, and CD, respectively, which is 9.8%, 1.8%, 2.0%, 3.9%, and 11.9% higher than

that in the Base scenario (Figure 7 (b), Table S8). The mean diurnal $|\Delta O_3|$ at ZL site (29.1 ppb,

38.2%) in the Free scenario was significantly higher compared to that of the Base scenario, followed

by XD (19.8 ppb, 6.4%), TZ (13.1 ppb, 6.2%) and CQ (18.1 ppb, 0.6%) (Figure 7 (c), Table S8),

suggesting that the absence of OVOCs constraint in OBM can significantly bias the O_3 formation

analysis in urban and industrial areas with complex emissions.

3.4 Uncertainty analysis

The uncertainty of the model mainly comes from the setting of NO_x (Text S1). Sensitive model

runs are performed with different NO_x settings to show the corresponding uncertainty. Firstly, NO_{ss},

$[NO_2]_{cor}$, VOCs, OVOCs, T, RH, and BLH are constrained in the Base scenario, and sensitivity

simulations were carried out for gradient NO_2 mixing ratios (50%, 60%, 70% of $[NO_2]_{obs}$). Generally,

different NO_2 settings produce uncertainties of -12%~7% for daytime O_3 and -30%~10% for the

daytime $R_{NetProd}$ of OVOCs. In addition, different NO_2 settings produce uncertainties of -122%~14%

for the $R_{Emis\&Trans}$ of OVOCs. This indicates that reducing the uncertainty of NO_2 observations is

important for further atmospheric chemistry modelling. Secondly, the $[NO]_{ss}$ and observed NO

mixing ratio ($[NO]_{obs}$) was respectively used in the model to investigate the influence of nearby NO

emissions on the OBM result (Table S3). Sensitivity tests show that directly using the $[NO]_{obs}$ may

resulted in an uncertainty of 3% ~20%, 10% ~27% and 7.1%~38% for O_3, $R_{NetProd}$ and $R_{Emis\&Trans}$,

respectively, with significantly higher uncertainties at TZ than at other stations, which may be

458   related to the strong transient emissions of NO_x.

459   The OH radicals are the main oxidant in the atmospheric troposphere. Most trace gases (CO,

460   CH_4 and VOCs) react with OH to produce peroxyl radicals, including HO_2, and RO_2. Peroxyl

461   radicals then react with NO to promote O_3. Photolysis of HONO is one of the important sources of

462   OH radicals. However, direct measurement of HONO was not conducted in this study. The input of

463   HONO in this study used the value of linear relationship with NO_2 mixing ratios, which may cause

464   some uncertainty. Sensitivity analyses were conducted based on the typical urban site (ZL) to

465   quantify the effect of different $HONO/NO_2$ ratios on free radicals and O_3. As shown in Figure S12,

466   as the ratio of $HONO/NO_2$ increased, the mixing ratio of HONO increased, and the concentration

467   of OH produced by photolysis of HONO increased. At the same time, the peroxyl radical and O_3

468   concentrations also increased (Table S9). At the lowest $HONO/NO_2$ ratio (0.005), the daytime OH,

469   HO_2, RO_2, and O_3 levels decreased by 4.6%, 4.8%, 6.0%, and 3.4%, respectively, compared to the

470    $HONO/NO_2$ ratio of 0.02. On the contrary, at the highest $HONO/NO_2$ of 0.04, the daytime OH, HO_2,

471   RO_2, and O_3 levels increased by 5.4%, 5.6%, 7.2% and 3.8%, respectively, compared to the Base

472   case.

473   When analyzing the contribution of chemical pathways, emission/transport and deposition to

474   OVOCs according to Equations (1-3), the OVOC budget may be affected by the modeling time step.

475   A sensitivity analysis was conducted at ZL, with simulations at different time steps (30 min, 10 min ,

476   and 5 min). As shown in Figure S13, the diurnal trends of the chemical contributions ($R_{NetProd}$),

477   emission/transport ($R_{Emis\&Trans}$) and deposition (R_{Dep}) to OVOC are similar. The magnitude of the

478   instantaneous change in $R_{Emis\&Trans}$ decreases when the time step is shortened. Specifically, the

479   contributions of $R_{NetProd}$ and $R_{Emis\&Trans}$ to OVOC increased, while the contribution of R_{Dep} decreased

with shorter time steps (Table S10). When the time step was reduced to 5 minutes, the contributions of $R_{NetProd}$ and $R_{Emis\&Trans}$ to OVOC increased by 4.3% and 5.0%, respectively, while the contribution of R_{Dep} decreased by 0.2%. Therefore, shortening the time step in the model simulation may result in limited increase contribution from $R_{NetProd}$ and $R_{Emis\&Trans}$ to OVOC.

The OBM, while advantageous for its use of the near-explicit master chemical mechanism and its ability to reproduce atmospheric chemistry based on observations, has several inherent limitations. Firstly, it inadequately considers emission and transport processes (Wolfe et al., 2016), leading to uncertainties and potential biases in atmospheric chemical analysis. Future studies could differentiate the two processes using CTMs. Secondly, the steady-state assumption, which underpins OBM calculations, might become invalid in areas strongly influenced by nearby emissions (e.g., high-traffic and industrial intensive regions) (Wolfe et al., 2016). This may potentially cause overestimations of secondary products such as O_3, RO_x radicals, and OVOCs (Li et al., 2021, 2014b). In this study, simulations use NO_{ss} as inputs, acknowledging that traffic-related NO emissions may prevent the system from reaching an approximate steady state. The associated uncertainties have been discussed above. Lastly, the model may not fully capture all relevant chemical processes, such as heterogeneous reactions or the formation and the fate of intermediate species. For instance, the exclusion of $ClNO_2$ chemistry could result in underestimating RO_x and O_3 production in certain environments (Riedel et al., 2014; Xia et al., 2020). Future research should focus on refining the chemical mechanisms to better approximate real atmospheric conditions.

4. Conclusions

Compared with previous studies conducted in most Chinese cities, the VOCs level in Zibo is in the upper-middle range (>32 ppb), with OVOCs being the second-largest contributor

502   (29.4%~36.1%) after alkanes (34.8%~53.3%). Higher levels of OVOCs were observed at sites with

503   more prominent emissions, with mixing ratios ranked as suburban (TZ, 19.7 ppb) > industrial (XD,

504   16.8 ppb) > urban (ZL, 14.9 ppb) > upwind (CQ, 13.9 ppb) > downwind (CD, 10.4 ppb). The OFP

505   in Zibo is 410.4±197.2 $\mu g\ m^{-3}$, with OVOCs accounting for the largest proportion (31.5%~55.9%).

506   The upwind site (CQ, 464.2±162.3 $\mu g\ m^{-3}$) has the highest OFP, followed by the suburban site (TZ,

507   456.3±295.3 $\mu g\ m^{-3}$), the urban site (ZL, 441.1±174.5 $\mu g\ m^{-3}$), the industrial site (XD, 422.9±166.9

508   $\mu g\ m^{-3}$), and the downwind site (CD, 279.4±101.2 $\mu g\ m^{-3}$) (Table S5). OFP contributed by OVOCs

509   is most dominant at suburban (TZ, 254.9 $\mu g\ m^{-3}$) and industrial (XD, 194.7 $\mu g\ m^{-3}$) sites, followed

510   by urban (ZL, 148.9 $\mu g\ m^{-3}$), upwind (CQ, 146.2 $\mu g\ m^{-3}$), and downwind (CD, 102.3 $\mu g\ m^{-3}$) sites.

511   The high levels of OVOCs and their significant contribution to OFP highlights their crucial role in

512   O_3 production across the observing stations.

513   Based on the OBM simulation, daytime OVOCs primarily originate from photochemical

514   generation, while at nighttime, emissions/transport is the main sources. This diurnal pattern is

515   closely related to the cyclical nature of human activities in urban areas (ZL), where stronger human

516   activities such as vehicle emissions in the daytime enhance the secondary generation of OVOCs.

517   Conversely, in industrial and suburban areas (XD, CQ, and TZ), emissions/transports dominate

518   nighttime OVOC levels, leading to higher mixing ratios at night compared to the daytime.

519   Without OVOCs constraint in the OBM, OVOCs are overestimated by 42.1%~126.5% in the

520   Free scenario. The impact of OVOCs constraint on $P(RO_x)$ is most significant at the urban site (ZL)

521   (29.4%), comparable to downwind site (CD) (27.6%), and higher than the industrial site (XD)

522   (17.8%), upwind site (CQ) (15.8%) and suburban site (TZ) (4.7%). In addition, this overestimation

523   of OVOCs in the Free scenario accelerates the reaction of OH with OVOCs and the photolysis of

OVOCs, promoting increased production of RO_2 (6.6%~35.1%) and HO_2 (5.3%~ 20.4%), which in turn leads to an overestimation of O_3 (1.8%~11.9%) during the daytime. However, the reaction rates of OH with OVOCs are overestimated without OVOCs constraint, which leads to underestimation of OH (3.4%~12.7%) and AOC (0.1%~10.0%). Therefore, to minimize the bias of numerical models, particularly in areas with complex anthropogenic activities, it is essential to intensify OVOCs observations and integrate them into numerical models. These efforts are crucial for refining atmospheric photochemistry simulation, improving the accuracy of O_3 formation predictions, and formulating more effective air quality management strategies for regions experiencing similar pollution challenges.

Author contributions

KZ, XY, RL, JX, QL, LSS, JQL, YNY, FTW and LMY conducted the field measurements. JWD and KZ performed the data analysis and prepared the manuscript with contributions from all co-authors. KZ, YLF, HC, LH, JNT, YJW and LL reviewed and edited the manuscript. All authors contributed to data interpretation and discussions.

Competing interests

The contact author has declared that none of the authors has any competing interests.

Acknowledgment

This study was financially supported by the National research program for key issues in air pollution control (DQGG202119). This work is supported by Shanghai Technical Service Center of Science and Engineering Computing, Shanghai University.

References

Armstrong, R. A., Slade, S. V., and Eperjesi, F.: An introduction to analysis of variance (ANOVA) with special reference to data from clinical experiments in optometry, Ophthalmic and

547   Physiological Optics, 20, 235–241, https://doi.org/10.1046/j.1475-1313.2000.00502.x, 2000.

548   Atkinson, R.: Atmospheric chemistry of VOCs and NOx, Atmos. Environ., 34, 2063–2101,

549   https://doi.org/10.1016/S1352-2310(99)00460-4, 2000.

550   Atkinson, R. and Arey, J.: Atmospheric Degradation of Volatile Organic Compounds, Chem. Rev.,

551   103, 4605–4638, https://doi.org/10.1021/cr0206420, 2003.

552   Bufalini, J. J. and Dodge, M. C.: Ozone-forming potential of light saturated hydrocarbons, Environ.

553   Sci. Technol., 17, 308–311, https://doi.org/10.1021/es00111a013, 1983.

554   Carter, W.: Updated maximum incremental reactivity scale and hydrocarbon bin reactivities for

555   regulatory applications, California Air Resources Board Contract, 1, 07–339, 2010a.

556   Carter, W. P. L.: A detailed mechanism for the gas-phase atmospheric reactions of organic

557   compounds, Atmospheric Environment. Part A. General Topics, 24, 481–518,

558   https://doi.org/10.1016/0960-1686(90)90005-8, 1990.

559   Carter, W. P. L.: Development of the SAPRC-07 chemical mechanism, Atmos. Environ., 44, 5324–

560   5335, https://doi.org/10.1016/j.atmosenv.2010.01.026, 2010b.

561   Carter, W. P. L. and Heo, G.: Development of revised SAPRC aromatics mechanisms, Atmos.

562   Environ., 77, 404–414, https://doi.org/10.1016/j.atmosenv.2013.05.021, 2013.

563   Chen, T., Xue, L., Zheng, P., Zhang, Y., Liu, Y., Sun, J., Han, G., Li, H., Zhang, X., Li, Y., Li, H.,

564   Dong, C., Xu, F., Zhang, Q., and Wang, W.: Volatile organic compounds and ozone air pollution

565   in an oil production region in northern China, Atmos. Chem. Phys., 20, 7069–7086,

566   https://doi.org/10.5194/acp-20-7069-2020, 2020.

567   Chen, T., Zheng, P., Zhang, Y., Dong, C., Han, G., Li, H., Yang, X., Liu, Y., Sun, J., Li, H., Zhang,

568   X., Li, Y., Wang, W., and Xue, L.: Characteristics and formation mechanisms of atmospheric

569   carbonyls in an oilfield region of northern China, Atmos. Environ., 274, 118958,

570   https://doi.org/10.1016/j.atmosenv.2022.118958, 2022.

571   Del Negro, L. A., Fahey, D. W., Gao, R. S., Donnelly, S. G., Keim, E. R., Neuman, J. A., Cohen, R.

572   C., Perkins, K. K., Koch, L. C., Salawitch, R. J., Lloyd, S. A., Proffitt, M. H., Margitan, J. J.,

573   Stimpfle, R. M., Bonne, G. P., Voss, P. B., Wennberg, P. O., McElroy, C. T., Swartz, W. H.,

574   Kusterer, T. L., Anderson, D. E., Lait, L. R., and Bui, T. P.: Comparison of modeled and observed

575   values of NO_2 and JNO_2 during the Photochemistry of Ozone Loss in the Arctic Region in

576   Summer (POLARIS) mission, J. Geophys. Res.-Atmos., 104, 26687–26703,

577   https://doi.org/10.1029/1999JD900246, 1999.

578   Duan, J., Tan, J., Yang, L., Wu, S., and Hao, J.: Concentration, sources and ozone formation potential

579   of volatile organic compounds (VOCs) during ozone episode in Beijing, Atmospheric Research,

580   88, 25–35, https://doi.org/10.1016/j.atmosres.2007.09.004, 2008.

581   Edwards, P. M., Brown, S. S., Roberts, J. M., Ahmadov, R., Banta, R. M., deGouw, J. A., Dube, W.

582   P., Field, R. A., Flynn, J. H., Gilman, J. B., Graus, M., Helmig, D., Koss, A., Langford, A. O.,

583   Lefer, B. L., Lerner, B. M., Li, R., Li, S.-M., McKeen, S. A., Murphy, S. M., Parrish, D. D., Senff,

584   C. J., Soltis, J., Stutz, J., Sweeney, C., Thompson, C. R., Trainer, M. K., Tsai, C., Veres, P. R.,

585   Washenfelder, R. A., Warneke, C., Wild, R. J., Young, C. J., Yuan, B., and Zamora, R.: High

586   winter ozone pollution from carbonyl photolysis in an oil and gas basin, Nature, 514, 351–354,

587   https://doi.org/10.1038/nature13767, 2014.

588   Elshorbany, Y. F., Kurtenbach, R., Wiesen, P., Lissi, E., Rubio, M., Villena, G., Gramsch, E., Rickard,

589   A. R., Pilling, M. J., and Kleffmann, J.: Oxidation capacity of the city air of Santiago, Chile,

590   Atmos. Chem. Phys., 9, 2257–2273, https://doi.org/10.5194/acp-9-2257-2009, 2009.

Elshorbany, Y. F., Steil, B., Bruehl, C., and Lelieveld, J.: Impact of HONO on global atmospheric chemistry calculated with an empirical parameterization in the EMAC model, Atmos. Chem. Phys., 12, 9977–10000, https://doi.org/10.5194/acp-12-9977-2012, 2012.

Emmerson, K. M., Carslaw, N., and Pilling, M. J.: Urban atmospheric chemistry during the PUMA campaign 2: Radical budgets for OH, HO_2 and RO_2, J. Atmos. Chem., 52, 165–183, https://doi.org/10.1007/s10874-005-1323-2, 2005.

Fuchs, H., Tan, Z., Lu, K., Bohn, B., Broch, S., Brown, S. S., Dong, H., Gomm, S., Häseler, R., He, L., Hofzumahaus, A., Holland, F., Li, X., Liu, Y., Lu, S., Min, K.-E., Rohrer, F., Shao, M., Wang, B., Wang, M., Wu, Y., Zeng, L., Zhang, Y., Wahner, A., and Zhang, Y.: OH reactivity at a rural site (Wangdu) in the North China Plain: contributions from OH reactants and experimental OH budget, Atmos. Chem. Phys., 17, 645–661, https://doi.org/10.5194/acp-17-645-2017, 2017.

Gentner, D. R., Worton, D. R., Isaacman, G., Davis, L. C., Dallmann, T. R., Wood, E. C., Herndon, S. C., Goldstein, A. H., and Harley, R. A.: Chemical Composition of Gas-Phase Organic Carbon Emissions from Motor Vehicles and Implications for Ozone Production, Environ. Sci. Technol., 47, 11837–11848, https://doi.org/10.1021/es401470e, 2013.

Geyer, A., Alicke, B., Konrad, S., Schmitz, T., Stutz, J., and Platt, U.: Chemistry and oxidation capacity of the nitrate radical in the continental boundary layer near Berlin, J. Geophys. Res.-Atmos., 106, 8013–8025, https://doi.org/10.1029/2000JD900681, 2001.

Gilman, J. B., Lerner, B. M., Kuster, W. C., Goldan, P. D., Warneke, C., Veres, P. R., Roberts, J. M., de Gouw, J. A., Burling, I. R., and Yokelson, R. J.: Biomass burning emissions and potential air quality impacts of volatile organic compounds and other trace gases from fuels common in the US, Atmos. Chem. Phys., 15, 13915–13938, https://doi.org/10.5194/acp-15-13915-2015, 2015.

Goldan, P. D., Kuster, W. C., Williams, E., Murphy, P. C., Fehsenfeld, F. C., and Meagher, J.: Nonmethane hydrocarbon and oxy hydrocarbon measurements during the 2002 New England Air Quality Study, J. Geophys. Res.-Atmos., 109, D21309, https://doi.org/10.1029/2003JD004455, 2004.

Goliff, W. S., Stockwell, W. R., and Lawson, C. V.: The regional atmospheric chemistry mechanism, version 2, Atmos. Environ., 68, 174–185, https://doi.org/10.1016/j.atmosenv.2012.11.038, 2013.

de Gouw, J. A., Gilman, J. B., Kim, S.-W., Alvarez, S. L., Dusanter, S., Graus, M., Griffith, S. M., Isaacman-VanWertz, G., Kuster, W. C., Lefer, B. L., Lerner, B. M., McDonald, B. C., Rappenglück, B., Roberts, J. M., Stevens, P. S., Stutz, J., Thalman, R., Veres, P. R., Volkamer, R., Warneke, C., Washenfelder, R. A., and Young, C. J.: Chemistry of Volatile Organic Compounds in the Los Angeles Basin: Formation of Oxygenated Compounds and Determination of Emission Ratios, Journal of Geophysical Research: Atmospheres, 123, 2298–2319, https://doi.org/10.1002/2017JD027976, 2018.

Guo, F., Bui, A. A. T., Schulze, B. C., Yoon, S., Shrestha, S., Wallace, H. W., Sakai, Y., Actkinson, B. W., Erickson, M. H., Alvarez, S., Sheesley, R., Usenko, S., Flynn, J., and Griffin, R. J.: Urban core-downwind differences and relationships related to ozone production in a major urban area in Texas, Atmos. Environ., 262, 118624, https://doi.org/10.1016/j.atmosenv.2021.118624, 2021.

Han, Y., Huang, X., Wang, C., Zhu, B., and He, L.: Characterizing oxygenated volatile organic compounds and their sources in rural atmospheres in China, J. Environ. Sci., 81, 148–155, https://doi.org/10.1016/j.jes.2019.01.017, 2019.

Huang, X.-F., Zhang, B., Xia, S.-Y., Han, Y., Wang, C., Yu, G.-H., and Feng, N.: Sources of oxygenated volatile organic compounds (OVOCs) in urban atmospheres in North and South

635   China, Environ. Pollut., 261, 114152, https://doi.org/10.1016/j.envpol.2020.114152, 2020.

636 Jenkin, M. E., Young, J. C., and Rickard, A. R.: The MCM v3.3.1 degradation scheme for isoprene,
637   Atmos. Chem. Phys., 15, 11433–11459, https://doi.org/10.5194/acp-15-11433-2015, 2015.

638 Jiang, P., Chen, X., Li, Q., Mo, H., and Li, L.: High-resolution emission inventory of gaseous and
639   particulate pollutants in Shandong Province, eastern China, Journal of Cleaner Production, 259,
640   120806, https://doi.org/10.1016/j.jclepro.2020.120806, 2020.

641 Kanaya, Y., Pochanart, P., Liu, Y., Li, J., Tanimoto, H., Kato, S., Suthawaree, J., Inomata, S.,
642   Taketani, F., Okuzawa, K., Kawamura, K., Akimoto, H., and Wang, Z. F.: Rates and regimes of
643   photochemical ozone production over Central East China in June 2006: a box model analysis
644   using comprehensive measurements of ozone precursors, Atmos. Chem. Phys., 9, 7711–7723,
645   https://doi.org/10.5194/acp-9-7711-2009, 2009.

646 Karl, T., Striednig, M., Graus, M., Hammerle, A., and Wohlfahrt, G.: Urban flux measurements
647   reveal a large pool of oxygenated volatile organic compound emissions, Proc. Natl. Acad. Sci. U.
648   S. A., 115, 1186–1191, https://doi.org/10.1073/pnas.1714715115, 2018.

649 Karl, T. G., Christian, T. J., Yokelson, R. J., Artaxo, P., Hao, W. M., and Guenther, A.: The Tropical
650   Forest and Fire Emissions Experiment: method evaluation of volatile organic compound
651   emissions measured by PTR-MS, FTIR, and GC from tropical biomass burning, Atmos. Chem.
652   Phys., 7, 5883–5897, https://doi.org/10.5194/acp-7-5883-2007, 2007.

653 Kim, S., Kim, S.-Y., Lee, M., Shim, H., Wolfe, G. M., Guenther, A. B., He, A., Hong, Y., and Han,
654   J.: Impact of isoprene and HONO chemistry on ozone and OVOC formation in a semirural South
655   Korean forest, Atmos. Chem. Phys., 15, 4357–4371, https://doi.org/10.5194/acp-15-4357-2015,
656   2015.

657 Koss, A. R., de Gouw, J., Warneke, C., Gilman, J. B., Lerner, B. M., Graus, M., Yuan, B., Edwards,
658   P., Brown, S. S., Wild, R., Roberts, J. M., Bates, T. S., and Quinn, P. K.: Photochemical aging of
659   volatile organic compounds associated with oil and natural gas extraction in the Uintah Basin,
660   UT, during a wintertime ozone formation event, Atmos. Chem. Phys., 15, 5727–5741,
661   https://doi.org/10.5194/acp-15-5727-2015, 2015.

662 Legreid, G., Reimann, S., Steinbacher, M., Staehelin, J., Young, D., and Stemmler, K.:
663   Measurements of OVOCs and NMHCs in a swiss highway tunnel for estimation of road transport
664   emissions, Environ. Sci. Technol., 41, 7060–7066, https://doi.org/10.1021/es062309+, 2007.

665 Li, B., Yu, S., Shao, M., Li, X., Ho, S. S. H., Hu, X., Wang, H., Feng, R., and Fang, X.: New insights
666   into photochemical initial concentrations of VOCs and their source implications, Atmos. Environ.,
667   298, 119616, https://doi.org/10.1016/j.atmosenv.2023.119616, 2023.

668 Li, C., Liu, Y., Cheng, B., Zhang, Y., Liu, X., Qu, Y., An, J., Kong, L., Zhang, Y., Zhang, C., Tan,
669   Q., and Feng, M.: A comprehensive investigation on volatile organic compounds (VOCs) in 2018
670   in Beijing, China: Characteristics, sources and behaviours in response to O_3 formation, Sci. Total
671   Environ., 806, 150247, https://doi.org/10.1016/j.scitotenv.2021.150247, 2022a.

672 Li, H., Ma, Y., Duan, F., He, K., Zhu, L., Huang, T., Kimoto, T., Ma, X., Ma, T., Xu, L., Xu, B.,
673   Yang, S., Ye, S., Sun, Z., An, J., and Zhang, Z.: Typical winter haze pollution in Zibo, an industrial
674   city in China: Characteristics, secondary formation, and regional contribution, Environmental
675   Pollution, 229, 339–349, https://doi.org/10.1016/j.envpol.2017.05.081, 2017.

676 Li, J., Xie, X., Li, L., Wang, X., Wang, H., Jing, S., Ying, Q., Qin, M., and Hu, J.: Fate of Oxygenated
677   Volatile Organic Compounds in the Yangtze River Delta Region: Source Contributions and
678   Impacts on the Atmospheric Oxidation Capacity, Environ. Sci. Technol., 56, 11212–11224,

679 https://doi.org/10.1021/acs.est.2c00038, 2022b.

680 Li, K., Wang, X., Li, L., Wang, J., Liu, Y., Cheng, X., Xu, B., Wang, X., Yan, P., Li, S., Geng, C.,
681 Yang, W., Azzi, M., and Bai, Z.: Large variability of O_3-precursor relationship during severe
682 ozone polluted period in an industry-driven cluster city (Zibo) of North China Plain, J. Clean
683 Prod., 316, 128252, https://doi.org/10.1016/j.jclepro.2021.128252, 2021a.

684 Li, K., Jacob, D. J., Liao, H., Qiu, Y., Shen, L., Zhai, S., Bates, K. H., Sulprizio, M. P., Song, S., Lu,
685 X., Zhang, Q., Zheng, B., Zhang, Y., Zhang, J., Lee, H. C., and Kuk, S. K.: Ozone pollution in
686 the North China Plain spreading into the late-winter haze season, Proc. Natl. Acad. Sci. U. S. A.,
687 118, e2015797118, https://doi.org/10.1073/pnas.2015797118, 2021b.

688 Li, L., Chen, Y., Zeng, L., Shao, M., Xie, S., Chen, W., Lu, S., Wu, Y., and Cao, W.: Biomass burning
689 contribution to ambient volatile organic compounds (VOCs) in the Chengdu-Chongqing Region
690 (CCR), China, Atmos. Environ., 99, 403–410, https://doi.org/10.1016/j.atmosenv.2014.09.067,
691 2014a.

692 Li, M., Zhang, Q., Streets, D. G., He, K. B., Cheng, Y. F., Emmons, L. K., Huo, H., Kang, S. C., Lu,
693 Z., Shao, M., Su, H., Yu, X., and Zhang, Y.: Mapping Asian anthropogenic emissions of non-
694 methane volatile organic compounds to multiple chemical mechanisms, Atmos. Chem. Phys., 14,
695 5617–5638, https://doi.org/10.5194/acp-14-5617-2014, 2014b.

696 Li, M., Zhang, Q., Zheng, B., Tong, D., Lei, Y., Liu, F., Hong, C., Kang, S., Yan, L., Zhang, Y., Bo,
697 Y., Su, H., Cheng, Y., and He, K.: Persistent growth of anthropogenic non-methane volatile
698 organic compound (NMVOC) emissions in China during 1990-2017: drivers, speciation and
699 ozone formation potential, Atmos. Chem. Phys., 19, 8897–8913, https://doi.org/10.5194/acp-19-
700 8897-2019, 2019.

701 Li, X., Rohrer, F., Brauers, T., Hofzumahaus, A., Lu, K., Shao, M., Zhang, Y. H., and Wahner, A.:
702 Modeling of HCHO and CHOCHO at a semi-rural site in southern China during the PRIDE-
703 PRD2006 campaign, Atmos. Chem. Phys., 14, 12291–12305, https://doi.org/10.5194/acp-14-
704 12291-2014, 2014c.

705 Ling, Z. H., Guo, H., Lam, S. H. M., Saunders, S. M., and Wang, T.: Atmospheric photochemical
706 reactivity and ozone production at two sites in Hong Kong: Application of a Master Chemical
707 Mechanism–photochemical box model, J. Geophys. Res.-Atmos., 119, 10567–10582,
708 https://doi.org/10.1002/2014JD021794, 2014.

709 Liu, G., Ma, X., Li, W., Chen, J., Ji, Y., and An, T.: Pollution characteristics, source appointment
710 and environmental effect of oxygenated volatile organic compounds in Guangdong-Hong Kong-
711 Macao Greater Bay Area: Implication for air quality management, Sci. Total Environ., 919,
712 170836, https://doi.org/10.1016/j.scitotenv.2024.170836, 2024.

713 Liu, T., Hong, Y., Li, M., Xu, L., Chen, J., Bian, Y., Yang, C., Dan, Y., Zhang, Y., Xue, L., Zhao, M.,
714 Huang, Z., and Wang, H.: Atmospheric oxidation capacity and ozone pollution mechanism in a
715 coastal city of southeastern China: analysis of a typical photochemical episode by an observation-
716 based model, Atmos. Chem. Phys., 22, 2173–2190, https://doi.org/10.5194/acp-22-2173-2022,
717 2022.

718 Liu, Y., Yuan, B., Li, X., Shao, M., Lu, S., Li, Y., Chang, C.-C., Wang, Z., Hu, W., Huang, X., He,
719 L., Zeng, L., Hu, M., and Zhu, T.: Impact of pollution controls in Beijing on atmospheric
720 oxygenated volatile organic compounds (OVOCs) during the 2008 Olympic Games: observation
721 and modeling implications, Atmos. Chem. Phys., 15, 3045–3062, https://doi.org/10.5194/acp-15-
722 3045-2015, 2015.

Liu, Z., Wang, Y., Gu, D., Zhao, C., Huey, L. G., Stickel, R., Liao, J., Shao, M., Zhu, T., Zeng, L., Amoroso, A., Costabile, F., Chang, C.-C., and Liu, S.-C.: Summertime photochemistry during CAREBeijing-2007: RO_x budgets and O_3 formation, Atmos. Chem. Phys., 12, 7737–7752, https://doi.org/10.5194/acp-12-7737-2012, 2012.

Liu, Z., Wang, Y., Hu, B., Lu, K., Tang, G., Ji, D., Yang, X., Gao, W., Xie, Y., Liu, J., Yao, D., Yang, Y., and Zhang, Y.: Elucidating the quantitative characterization of atmospheric oxidation capacity in Beijing, China, Sci. Total Environ., 771, 145306, https://doi.org/10.1016/j.scitotenv.2021.145306, 2021.

Lou, S., Holland, F., Rohrer, F., Lu, K., Bohn, B., Brauers, T., Chang, C. C., Fuchs, H., Haeseler, R., Kita, K., Kondo, Y., Li, X., Shao, M., Zeng, L., Wahner, A., Zhang, Y., Wang, W., and Hofzumahaus, A.: Atmospheric OH reactivities in the Pearl River Delta - China in summer 2006: measurement and model results, Atmos. Chem. Phys., 10, 11243–11260, https://doi.org/10.5194/acp-10-11243-2010, 2010.

Luecken, D. J., Hutzell, W. T., Strum, M. L., and Pouliot, G. A.: Regional sources of atmospheric formaldehyde and acetaldehyde, and implications for atmospheric modeling, Atmos. Environ., 47, 477–490, https://doi.org/10.1016/j.atmosenv.2011.10.005, 2012.

McDonald, B. C., de Gouw, J. A., Gilman, J. B., Jathar, S. H., Akherati, A., Cappa, C. D., Jimenez, J. L., Lee-Taylor, J., Hayes, P. L., McKeen, S. A., Cui, Y. Y., Kim, S.-W., Gentner, D. R., Isaacman-VanWertz, G., Goldstein, A. H., Harley, R. A., Frost, G. J., Roberts, J. M., Ryerson, T. B., and Trainer, M.: Volatile chemical products emerging as largest petrochemical source of urban organic emissions, Science, 359, 760–764, https://doi.org/10.1126/science.aaq0524, 2018.

Mo, Z., Shao, M., and Lu, S.: Compilation of a source profile database for hydrocarbon and OVOC emissions in China, Atmos. Environ., 143, 209–217, https://doi.org/10.1016/j.atmosenv.2016.08.025, 2016.

Mo, Z., Shao, M., Wang, W., Liu, Y., Wang, M., and Lu, S.: Evaluation of biogenic isoprene emissions and their contribution to ozone formation by ground-based measurements in Beijing, China, Sci. Total Environ., 627, 1485–1494, https://doi.org/10.1016/j.scitotenv.2018.01.336, 2018.

Mo, Z., Huang, S., Yuan, B., Pei, C., Song, Q., Qi, J., Wang, M., Wang, B., Wang, C., and Shao, M.: Tower-based measurements of NMHCs and OVOCs in the Pearl River Delta: Vertical distribution, source analysis and chemical reactivity, Environ. Pollut., 292, 118454, https://doi.org/10.1016/j.envpol.2021.118454, 2022.

Ou, J., Zheng, J., Li, R., Huang, X., Zhong, Z., Zhong, L., and Lin, H.: Speciated OVOC and VOC emission inventories and their implications for reactivity-based ozone control strategy in the Pearl River Delta region, China, Sci. Total Environ., 530, 393–402, https://doi.org/10.1016/j.scitotenv.2015.05.062, 2015.

Peng, Y., Cai, J., Feng, Y., Jiang, H., and Chen, Y.: Emission characteristic of OVOCs, I/SVOCs, OC and EC from wood combustion at different moisture contents, Atmos. Environ., 298, 119620, https://doi.org/10.1016/j.atmosenv.2023.119620, 2023.

Pfannerstill, E. Y., Arata, C., Zhu, Q., Schulze, B. C., Woods, R., Harkins, C., Schwantes, R. H., McDonald, B. C., Seinfeld, J. H., Bucholtz, A., Cohen, R. C., and Goldstein, A. H.: Comparison between Spatially Resolved Airborne Flux Measurements and Emission Inventories of Volatile Organic Compounds in Los Angeles, Environ. Sci. Technol., 57, 15533–15545, https://doi.org/10.1021/acs.est.3c03162, 2023.

Qin, Z., Xu, B., Zheng, Z., Li, L., Zhang, G., Li, S., Geng, C., Bai, Z., and Yang, W.: Integrating ambient carbonyl compounds provides insight into the constrained ozone formation chemistry in Zibo city of the North China Plain, Environ. Pollut., 324, 121294, https://doi.org/10.1016/j.envpol.2023.121294, 2023.

Qu, H., Wang, Y., Zhang, R., Liu, X., Huey, L. G., Sjostedt, S., Zeng, L., Lu, K., Wu, Y., Shao, M., Hu, M., Tan, Z., Fuchs, H., Broch, S., Wahner, A., Zhu, T., and Zhang, Y.: Chemical Production of Oxygenated Volatile Organic Compounds Strongly Enhances Boundary-Layer Oxidation Chemistry and Ozone Production, Environ. Sci. Technol., 55, 13718–13727, https://doi.org/10.1021/acs.est.1c04489, 2021.

Ren, Q.: Circular economy action programs and countermeasures for small and medium-sized resource-based cities of China-case study of Zibo City of Shandong Province, Energy Procedia, 2183–2188, https://doi.org/10.1016/j.egypro.2011.03.377, 2011.

Rieksta, J., Li, T., Davie-Martin, C. L., Aeppli, L. C. B., Hoye, T. T., and Rinnan, R.: Volatile responses of dwarf birch to mimicked insect herbivory and experimental warming at two elevations in Greenlandic tundra., Plant Environ Interact, 4, 23–35, https://doi.org/10.1002/pei3.10100, 2023.

Sarwar, G., Luecken, D., Yarwood, G., Whitten, G. Z., and Carter, W. P. L.: Impact of an updated carbon bond mechanism on predictions from the CMAQ modeling system: Preliminary assessment, J. Appl. Meteorol. Climatol., 47, 3–14, https://doi.org/10.1175/2007JAMC1393.1, 2008.

Saunders, S. M., Jenkin, M. E., Derwent, R. G., and Pilling, M. J.: Protocol for the development of the Master Chemical Mechanism, MCM v3 (Part A): tropospheric degradation of non-aromatic volatile organic compounds, Atmos. Chem. Phys., 3, 161–180, https://doi.org/10.5194/acp-3-161-2003, 2003.

Shen, L., Jacob, D. J., Zhu, L., Zhang, Q., Zheng, B., Sulprizio, M. P., Li, K., De Smedt, I., Abad, G. G., Cao, H., Fu, T.-M., and Liao, H.: The 2005-2016 Trends of Formaldehyde Columns Over China Observed by Satellites: Increasing Anthropogenic Emissions of Volatile Organic Compounds and Decreasing Agricultural Fire Emissions, Geophys. Res. Lett., 46, 4468–4475, https://doi.org/10.1029/2019GL082172, 2019.

Sindelarova, K., Granier, C., Bouarar, I., Guenther, A., Tilmes, S., Stavrakou, T., Muller, J.-F., Kuhn, U., Stefani, P., and Knorr, W.: Global data set of biogenic VOC emissions calculated by the MEGAN model over the last 30 years, Atmos. Chem. Phys., 14, 9317–9341, https://doi.org/10.5194/acp-14-9317-2014, 2014.

Song, J., Saathoff, H., Jiang, F., Gao, L., Zhang, H., and Leisner, T.: Sources of organic gases and aerosol particles and their roles in nighttime particle growth at a rural forested site in southwest Germany, Atmos. Chem. Phys., 24, 6699–6717, https://doi.org/10.5194/acp-24-6699-2024, 2024.

Song, M., Li, X., Yang, S., Yu, X., Zhou, S., Yang, Y., Chen, S., Dong, H., Liao, K., Chen, Q., Lu, K., Zhang, N., Cao, J., Zeng, L., and Zhang, Y.: Spatiotemporal variation, sources, and secondary transformation potential of volatile organic compounds in Xi'an, China, Atmos. Chem. Phys., 21, 4939–4958, https://doi.org/10.5194/acp-21-4939-2021, 2021.

Steiner, A. L., Cohen, R. C., Harley, R. A., Tonse, S., Millet, D. B., Schade, G. W., and Goldstein, A. H.: VOC reactivity in central California: comparing an air quality model to ground-based measurements, Atmos. Chem. Phys., 8, 351–368, https://doi.org/10.5194/acp-8-351-2008, 2008.

Stockwell, W. R., Kirchner, F., Kuhn, M., and Seefeld, S.: A new mechanism for regional

atmospheric chemistry modeling, J. Geophys. Res.-Atmos., 102, 25847–25879, https://doi.org/10.1029/97JD00849, 1997a.

Stockwell, W. R., Kirchner, F., Kuhn, M., and Seefeld, S.: A new mechanism for regional atmospheric chemistry modeling, J. Geophys. Res.-Atmos., 102, 25847–25879, https://doi.org/10.1029/97JD00849, 1997b.

Tan, Z., Fuchs, H., Lu, K., Hofzumahaus, A., Bohn, B., Broch, S., Dong, H., Gomm, S., Haeseler, R., He, L., Holland, F., Li, X., Liu, Y., Lu, S., Rohrer, F., Shao, M., Wang, B., Wang, M., Wu, Y., Zeng, L., Zhang, Y., Wahner, A., and Zhang, Y.: Radical chemistry at a rural site (Wangdu) in the North China Plain: observation and model calculations of OH, HO_2 and RO_2 radicals, Atmos. Chem. Phys., 17, 663–690, https://doi.org/10.5194/acp-17-663-2017, 2017.

Tan, Z., Lu, K., Jiang, M., Su, R., Dong, H., Zeng, L., Xie, S., Tan, Q., and Zhang, Y.: Exploring ozone pollution in Chengdu, southwestern China: A case study from radical chemistry to O_3-VOC-NO_x sensitivity, Sci. Total Environ., 636, 775–786, https://doi.org/10.1016/j.scitotenv.2018.04.286, 2018a.

Tan, Z., Rohrer, F., Lu, K., Ma, X., Bohn, B., Broch, S., Dong, H., Fuchs, H., Gkatzelis, G. I., Hofzumahaus, A., Holland, F., Li, X., Liu, Y., Liu, Y., Novelli, A., Shao, M., Wang, H., Wu, Y., Zeng, L., Hu, M., Kiendler-Scharr, A., Wahner, A., and Zhang, Y.: Wintertime photochemistry in Beijing: observations of RO_x radical concentrations in the North China Plain during the BEST-ONE campaign, Atmos. Chem. Phys., 18, 12391–12411, https://doi.org/10.5194/acp-18-12391-2018, 2018b.

Tan, Z., Lu, K., Jiang, M., Su, R., Wang, H., Lou, S., Fu, Q., Zhai, C., Tan, Q., Yue, D., Chen, D., Wang, Z., Xie, S., Zeng, L., and Zhang, Y.: Daytime atmospheric oxidation capacity in four Chinese megacities during the photochemically polluted season: a case study based on box model simulation, Atmos. Chem. Phys., 19, 3493–3513, https://doi.org/10.5194/acp-19-3493-2019, 2019a.

Tan, Z., Lu, K., Hofzumahaus, A., Fuchs, H., Bohn, B., Holland, F., Liu, Y., Rohrer, F., Shao, M., Sun, K., Wu, Y., Zeng, L., Zhang, Y., Zou, Q., Kiendler-Scharr, A., Wahner, A., and Zhang, Y.: Experimental budgets of OH, HO_2, and RO_2 radicals and implications for ozone formation in the Pearl River Delta in China 2014, Atmos. Chem. Phys., 19, 7129–7150, https://doi.org/10.5194/acp-19-7129-2019, 2019b.

Venecek, M. A., Carter, W. P. L., and Kleeman, M. J.: Updating the SAPRC Maximum Incremental Reactivity (MIR) scale for the United States from 1988 to 2010, J. Air Waste Manage. Assoc., 68, 1301–1316, https://doi.org/10.1080/10962247.2018.1498410, 2018.

Volkamer, R., Sheehy, P., Molina, L. T., and Molina, M. J.: Oxidative capacity of the Mexico City atmosphere - Part 1: A radical source perspective, Atmos. Chem. Phys., 10, 6969–6991, https://doi.org/10.5194/acp-10-6969-2010, 2010.

Wang, G., Zhu, Z., Liu, Z., Liu, X., Kong, F., Nie, L., Gao, W., Zhao, N., and Lang, J.: Ozone pollution in the plate and logistics capital of China: Insight into the formation, source apportionment, and regional transport, Environ. Pollut., 313, https://doi.org/10.1016/j.envpol.2022.120144, 2022a.

Wang, M., Zeng, L., Lu, S., Shao, M., Liu, X., Yu, X., Chen, W., Yuan, B., Zhang, Q., Hu, M., and Zhang, Z.: Development and validation of a cryogen-free automatic gas chromatograph system (GC-MS/FID) for online measurements of volatile organic compounds, Anal. Methods, 6, 9424–9434, https://doi.org/10.1039/C4AY01855A, 2014.

Wang, R., Wang, L., Yang, Y., Zhan, J., Ji, D., Hu, B., Ling, Z., Xue, M., Zhao, S., Yao, D., Liu, Y., and Wang, Y.: Comparative analysis for the impacts of VOC subgroups and atmospheric oxidation capacity on O_3 based on different observation-based methods at a suburban site in the North China Plain, Environ. Res., 248, 118250, https://doi.org/10.1016/j.envres.2024.118250, 2024.

Wang, S., Yuan, B., Wu, C., Wang, C., Li, T., He, X., Huangfu, Y., Qi, J., Li, X.-B., Sha, Q., Zhu, M., Lou, S., Wang, H., Karl, T., Graus, M., Yuan, Z., and Shao, M.: Oxygenated volatile organic compounds (VOCs) as significant but varied contributors to VOC emissions from vehicles, Atmos. Chem. Phys., 22, 9703–9720, https://doi.org/10.5194/acp-22-9703-2022, 2022b.

Wang, S., Zhang, J., Zhang, Y., Wang, L., Sun, Z., and Wang, H.: Review on Source Profiles of Volatile Organic Compounds (VOCs) in Typical Industries in China, Atmosphere, 14, 878, https://doi.org/10.3390/atmos14050878, 2023.

Wang, W., Yuan, B., Peng, Y., Su, H., Cheng, Y., Yang, S., Wu, C., Qi, J., Bao, F., Huangfu, Y., Wang, C., Ye, C., Wang, Z., Wang, B., Wang, X., Song, W., Hu, W., Cheng, P., Zhu, M., Zheng, J., and Shao, M.: Direct observations indicate photodearadable oxygenated volatile organic compounds (OVOCs) as larger contributors to radicals and ozone production in the atmosphere, Atmos. Chem. Phys., 22, 4117–4128, https://doi.org/10.5194/acp-22-4117-2022, 2022c.

Wolfe, G. M., Marvin, M. R., Roberts, S. J., Travis, K. R., and Liao, J.: The Framework for 0-D Atmospheric Modeling (F0AM) v3.1, Geosci. Model Dev., 9, 3309–3319, https://doi.org/10.5194/gmd-9-3309-2016, 2016.

Wu, Y., Fan, X., Liu, Y., Zhang, J., Wang, H., Sun, L., Fang, T., Mao, H., Hu, J., Wu, L., Peng, J., and Wang, S.: Source apportionment of VOCs based on photochemical loss in summer at a suburban site in Beijing, Atmos. Environ., 293, 119459, https://doi.org/10.1016/j.atmosenv.2022.119459, 2023.

Xia, S.-Y., Wang, C., Zhu, B., Chen, X., Feng, N., Yu, G.-H., and Huang, X.-F.: Long-term observations of oxygenated volatile organic compounds (OVOCs) in an urban atmosphere in southern China, 2014-2019, Environ. Pollut., 270, 116301, https://doi.org/10.1016/j.envpol.2020.116301, 2021.

Xu, Z., Wang, T., Xue, L. K., Louie, P. K. K., Luk, C. W. Y., Gao, J., Wang, S. L., Chai, F. H., and Wang, W. X.: Evaluating the uncertainties of thermal catalytic conversion in measuring atmospheric nitrogen dioxide at four differently polluted sites in China, Atmos. Environ., 76, 221–226, https://doi.org/10.1016/j.atmosenv.2012.09.043, 2013.

Xuan, H., Zhao, Y., Ma, Q., Chen, T., Liu, J., Wang, Y., Liu, C., Wang, Y., Liu, Y., Mu, Y., and He, H.: Formation mechanisms and atmospheric implications of summertime nitrous acid (HONO) during clean, ozone pollution and double high-level $PM_{2.5}$ and O_3 pollution periods in Beijing, Sci. Total Environ., 857, 159538, https://doi.org/10.1016/j.scitotenv.2022.159538, 2023.

Xue, L., Wang, T., Louie, P. K. K., Luk, C. W. Y., Blake, D. R., and Xu, Z.: Increasing External Effects Negate Local Efforts to Control Ozone Air Pollution: A Case Study of Hong Kong and Implications for Other Chinese Cities, Environ. Sci. Technol., 48, 10769–10775, https://doi.org/10.1021/es503278g, 2014a.

Xue, L., Gu, R., Wang, T., Wang, X., Saunders, S., Blake, D., Louie, P. K. K., Luk, C. W. Y., Simpson, I., Xu, Z., Wang, Z., Gao, Y., Lee, S., Mellouki, A., and Wang, W.: Oxidative capacity and radical chemistry in the polluted atmosphere of HongKong and Pearl River Delta region: analysis of a severe photochemical smog episode, Atmos. Chem. Phys., 16, 9891–9903,

https://doi.org/10.5194/acp-16-9891-2016, 2016.

Xue, L. K., Wang, T., Gao, J., Ding, A. J., Zhou, X. H., Blake, D. R., Wang, X. F., Saunders, S. M., Fan, S. J., Zuo, H. C., Zhang, Q. Z., and Wang, W. X.: Ground-level ozone in four Chinese cities: precursors, regional transport and heterogeneous processes, Atmos. Chem. Phys., 14, 13175–13188, https://doi.org/10.5194/acp-14-13175-2014, 2014b.

Yang, C., Yao, N., Xu, L., Chen, G., Wang, Y., Fan, X., Zhou, P., Clusius, P., Tham, Y. J., Lin, Z., Chen, Y., Li, M., Hong, Y., and Chen, J.: Molecular Composition of Anthropogenic Oxygenated Organic Molecules and Their Contribution to Organic Aerosol in a Coastal City, Environ. Sci. Technol., 57, 15956–15967, https://doi.org/10.1021/acs.est.3c03244, 2023.

Yang, M., Beale, R., Liss, P., Johnson, M., Blomquist, B., and Nightingale, P.: Air-sea fluxes of oxygenated volatile organic compounds across the Atlantic Ocean, Atmos. Chem. Phys., 14, 7499–7517, https://doi.org/10.5194/acp-14-7499-2014, 2014.

Yang, X., Xue, L., Wang, T., Wang, X., Gao, J., Lee, S., Blake, D. R., Chai, F., and Wang, W.: Observations and Explicit Modeling of Summertime Carbonyl Formation in Beijing: Identification of Key Precursor Species and Their Impact on Atmospheric Oxidation Chemistry, J. Geophys. Res.-Atmos., 123, 1426–1440, https://doi.org/10.1002/2017JD027403, 2018.

Yang, X., Cheng, X., Yan, H., Sun, Y., and Zhang, G.: Ground-Level Ozone Production over an Industrial Cluster of China: a Box Model Analysis of a Severe Photochemical Pollution Episode, Pol. J. Environ. Stud., 31, 1885–1899, https://doi.org/10.15244/pjoes/143253, 2022a.

Yang, X., Lu, K., Ma, X., Gao, Y., Tan, Z., Wang, H., Chen, X., Li, X., Huang, X., He, L., Tang, M., Zhu, B., Chen, S., Dong, H., Zeng, L., and Zhang, Y.: Radical chemistry in the Pearl River Delta: observations and modeling of OH and HO_2 radicals in Shenzhen in 2018, Atmos. Chem. Phys., 22, 12525–12542, https://doi.org/10.5194/acp-22-12525-2022, 2022b.

Yarwood, G., Rao, S., Way, R., Yocke, M., Whitten, G. Z., and Reyes, S.: Deborah Luecken U.S. Environmental Protection Agency Research Triangle Park, NC 27703, 2005.

Yarwood, G., Jung, J., Whitten, G. Z., Heo, G., Mellberg, J., and Estes, M.: Updates to the Carbon Bond mechanism for version 6 (CB6), 2010.

Yokelson, R. J., Karl, T., Artaxo, P., Blake, D. R., Christian, T. J., Griffith, D. W. T., Guenther, A., and Hao, W. M.: The Tropical Forest and Fire Emissions Experiment: overview and airborne fire emission factor measurements, Atmos. Chem. Phys., 7, 5175–5196, https://doi.org/10.5194/acp-7-5175-2007, 2007.

Zhang, K., Huang, L., Li, Q., Huo, J., Duan, Y., Wang, Y., Yaluk, E., Wang, Y., Fu, Q., and Li, L.: Explicit modeling of isoprene chemical processing in polluted air masses in suburban areas of the Yangtze River Delta region: radical cycling and formation of ozone and formaldehyde, Atmos. Chem. Phys., 21, 5905–5917, https://doi.org/10.5194/acp-21-5905-2021, 2021a.

Zhang, K., Duan, Y., Huo, J., Huang, L., Wang, Y., Fu, Q., Wang, Y., and Li, L.: Formation mechanism of HCHO pollution in the suburban Yangtze River Delta region, China: A box model study and policy implementations, Atmos. Environ., 267, 118755, https://doi.org/10.1016/j.atmosenv.2021.118755, 2021b.

Zhang, Z., Sun, Y., and Li, J.: Characteristics and sources of VOCs in a coastal city in eastern China and the implications in secondary organic aerosol and O_3 formation, Sci. Total Environ., 887, 164117, https://doi.org/10.1016/j.scitotenv.2023.164117, 2023.

Zheng, B., Zhang, Q., Geng, G., Chen, C., Shi, Q., Cui, M., Lei, Y., and He, K.: Changes in China's anthropogenic emissions and air quality during the COVID-19 pandemic in 2020, Earth Syst. Sci.

943   Data, 13, 2895–2907, https://doi.org/10.5194/essd-13-2895-2021, 2021.

944   Zheng, Z., Li, K., Xu, B., Dou, J., Li, L., Zhang, G., Li, S., Geng, C., Yang, W., Azzi, M., and Bai,
945   Z.: O_3-precursor relationship over multiple patterns of timescale: a case study in Zibo, Shandong
946   Province, China, Atmos. Chem. Phys., 23, 2649–2665, https://doi.org/10.5194/acp-23-2649-2023,
947   2023.

948   Zhou, J., Zhang, C., Liu, A., Yuan, B., Wang, Y., Wang, W., Zhou, J.-P., Hao, Y., Li, X.-B., He, X.,
949   Song, X., Chen, Y., Yang, S., Yang, S., Wu, Y., Jiang, B., Huang, S., Liu, J., Peng, Y., Qi, J., Deng,
950   M., Zhong, B., Huangfu, Y., and Shao, M.: Measurement report: Vertical and temporal variability
951   in the near-surface ozone production rate and sensitivity in an urban area in the Pearl River Delta
952   region, China, Atmos. Chem. Phys., 24, 9805–9826, https://doi.org/10.5194/acp-24-9805-2024,
953   2024.

954   Zhou, M., Jiang, W., Gao, W., Gao, X., Ma, M., and Ma, X.: Anthropogenic emission inventory of
955   multiple air pollutants and their spatiotemporal variations in 2017 for the Shandong Province,
956   China*, Environ. Pollut., 288, 117666, https://doi.org/10.1016/j.envpol.2021.117666, 2021.

957   Zhu, J., Wang, S., Wang, H., Jing, S., Lou, S., Saiz-Lopez, A., and Zhou, B.: Observationally
958   constrained modeling of atmospheric oxidation capacity and photochemical reactivity in
959   Shanghai, China, Atmos. Chem. Phys., 20, 1217–1232, https://doi.org/10.5194/acp-20-1217-
960   2020, 2020.

961